Lappeenranta University of Technology
School of Engineering Science
Degree Program in Technical Physics

Master's Thesis

Fadeev Egor

MAGNETIC PROPERTIES OF NI-CO-MN-IN HEUSLER ALLOYS

Examiners: Professor Erkki Lahderanta
D.Sc. Ivan Zakharchuk

ABSTRACT

Lappeenranta University of Technology
School of Engineering Science
Degree Program in Technical Physics

Fadeev Egor

Magnetic properties of Ni-Co-Mn-In Heusler alloys

Master's Thesis

2017

48 pages and 25 figures.

Examiners: Professor Erkki Lahderanta
D.Sc. Ivan Zakharchuk

Keywords: Heusler alloys, SQUID magnetometry, magnetocaloric effect, martensitic transition.

Magnetic properties and crystal structure of the bulk $Ni_{48.5}Co_{1.5}Mn_{35}In_{15}$ Heusler alloy have been investigated, using SQUID magnetometer and X-ray diffraction, respectively. Phase transition temperatures and their shift, under the influence of a change of magnetic field, have been detected, using magnetization versus temperature dependencies ($M(T)$). The magnetization dependencies on magnetic field ($M(H)$) at temperatures near to a martensitic transition temperature (T_M) have been measured, in order to evaluate the magnitude of a magnetocaloric effect, namely a magnetic entropy change (ΔS_m). Exchange bias (EB) phenomenon, that is attributed to ferromagnetic / antiferromagnetic coupling at low temperatures, has been observed during the $M(H)$ at T = 5 K after cooling in positive magnetic fields up to H = 5 T. The shift of hysteresis loop (H_E) is estimated as $H_E \approx$ 145 Oe. The magnetic entropy change reaches its maximum value of -32.1 $Jkg^{-1}K^{-1}$ at $T \approx 314$ K.

CONTENTS

ABBREVIATIONS AND SYMBOLS

FM / AFM	Ferromagnet / antiferromagnet
MCE	Magnetocaloric effect
EB	Exchange bias
AP / MP	Austenitic / martensitic phases
MT	Martensitic transition
FOPT	First order phase transition
SOPT	Second order phase transition
SQUID	Superconducting quantum interference device
VTI	Variable temperature insert
H	Magnetic field strength
M	Magnetization
B	Magnetic flux density
C	Curie constant
T_C	Curie point of austenitic phase
T_C^M	Curie point of martensitic phase
T_N	Neel temperature
T_M	Martensitic transition temperature
M_R	Residual magnetization
H_C	Coercive force
χ	Magnetic susceptibility
ΔS_m	Magnetic entropy change
ΔS_{lat}	Lattice entropy change
ΔT	Adiabatic temperature change
RC	Refrigerant capacity
TD	Temperature dependence
FD	Field dependence

1 INTRODUCTION

1.1 Background

Currently, the importance of the Heusler alloys investigations is dictated by their wide range of applications in spintronics. From the standpoint of spintronics, spin polarization of electrons play an important role. Theoretically, such alloys can demonstrate 100% spin polarization and can be used as spin-polarized electron sources along with metal oxides and III–V group semiconductors [1]. The history of Heusler alloys began in 1898, when the German physicist Friedrich Heusler discovered the presence of ferromagnetic properties in the fusion of nonmagnetic Mn, Cu, and Sn. However, at the present time in such materials we can observe not only ferromagnetism, but also antiferromagnetism, paramagnetism, diamagnetism, etc. Such effects as magnetic shape memory, magnetic field induced superelasticity, giant magnetoresistance, exchange bias, anomalous Hall effect and large strain induced changes in magnetization are among the most momentous fields of investigation. The Heusler alloys are promising materials for such devices as non-local spin-valves, magnetic tunnel junctions, spin injectors, etc [2].

The Heusler alloys exhibit a wide diversity of magnetic, electrical, optical, and mechanical properties important for fundamental research. It possesses a strong relationship between the structural and magnetic properties, and therefore, one can achieve different effects by variation of the chemical composition. Second important feature of Heusler alloys is combination of the first and second order phase transitions and the presence of temperature hysteresis during martensitic transition from the high-temperature cubic austenitic phase to the low-temperature tetragonal martensitic phase. The martensitic transition has been found experimentally in different Heusler alloys such as Ni-Mn-Ga, Ni-Fe-Ga, Co-Ni-Ga and others [3]. Over recent decades there was a significant rise of interest to magnetocaloric effect due to the possibility of its application in the technology of magnetic cooling in a wide range of temperatures. In the last years, refrigerators of a new generation are being developed on the basis of the magnetocaloric effect in order to eliminate the shortcomings of gas compressor refrigerators. Energy consumption of such refrigerators can be reduced to 20 - 30%. Moreover, the lack of any greenhouse effect related gases is a significant feature determining the importance of magnetocaloric effect study [4].

In addition, it is worth to emphasize the importance of exchange bias research due to wide range of promising devices working on this phenomenon such as permanent magnets,

domain stabilizers in recording heads, magnetic sensors, etc [5].

1.2 Objectives and restrictions

The aim of the thesis is the investigation of the magnetic properties of the $Ni_{48.5}Co_{1.5}Mn_{35}In_{15}$ Heusler alloy, namely, the study of the martensitic transition, the magnetocaloric effect, and the exchange bias. The work objectives are:

- Since the temperatures of the first and second order phase transitions in the Ni-Mn-based Heusler alloys strongly depend on the chemical composition, it is neccesary to estimate transition temperatures in the given sample [6–8]. For estimation one needs to measure magnetization as a function of temperature ($M(T)$) at different fields.
- To measure field dependencies ($M(H)$) at temperatures close to the martensitic transition temperature.
- To evaluate the magnitude of exchange bias shift at T = 5 K.
- Using the data from field dependencies, to calculate the magnetocaloric effect value, namely magnetic entropy change (ΔS_m).

The adiabatic temperatures change (ΔT_{ad}) and refrigerant capacity (RC) will not be estimated in this thesis.

1.3 Structure of the thesis

Chapter 2 briefly describes basic details about magnetism phenomenon and some imperative types of magnetic ordering. The structure and relevant properties of the Heusler alloys are represented in the third chapter. Chapter 4 contains description of the nature of different transition types. The explanation of the physical meaning of the magnetocaloric effect and the exchange bias phenomenon are shown in the chapters 5 and 6, respectively. The seventh chapter tells how to calculate three essential magnetocaloric effect parameters. Chapters 8 involve the description of structure and operation principle of a SQUID magnetometer. Explanations of obtained results is written in the chapter 9.

2 Nature of magnetism

Nowadays, magnetism in any substances is of great interest. There are five main types of magnetic ordering, associated with the concepts of diamagnetism, paramagnetism, ferromagnetism, antiferromagnetism and ferrimagnetism.

The substances which have a magnetic moment when placed in a magnetic field (magnetization process) are called magnets. Actually absolutely all materials are magnetized to some extent and, hence, can be considered as magnetic and categorized as weak (diamagnets or paramagnets) and strong (ferromagnets) magnetic.

Interpretation of magnetic phenomena in solids is based on two basic concepts. The first is that ions in a solid can have discrete magnetic moments. The induced moments are created by external magnetic fields. Spontaneous moments exist even in the absence of the external fields. The second idea is that these microscopic magnetic moments interact not only as ordinary dipoles (such forces are too weak to play an essential role), but they are also connected by the forces of quantum mechanical nature. So-called exchange forces depend on the distance between the magnetic ions, but also on their mutual geometric arrangement, and cause a variety of types of magnetic ordering in solids [9, 10].

2.1 Magnetization

The main magnetic characteristic of a substance is its magnetization, $\bar{M}$, which means a vector sum of all magnetic moments, $\bar{m}_i$, per unit volume

$$\bar{M} = \frac{1}{V} \sum_{i=1}^{N} \bar{m}_i \tag{1}$$

The magnetization is a function of the external magnetic field. The dependence is linear for many substances in a certain range of fields and temperatures (See Fig.1), i.e.

$$M = \chi H, \tag{2}$$

where χ is magnetic susceptibility and H is the external magnetic field. The susceptibility is negative for diamagnets and positive for paramagnets. The magnitude of susceptibility for both paramagnets and diamagnets is small, in range $10^{-4} - 10^{-6}$. In addition, there are strongly magnetic substances in which the magnetization is not a linear function of

the field, i.e., ferromagnets, ferrimagnets, antiferromagnets [11].

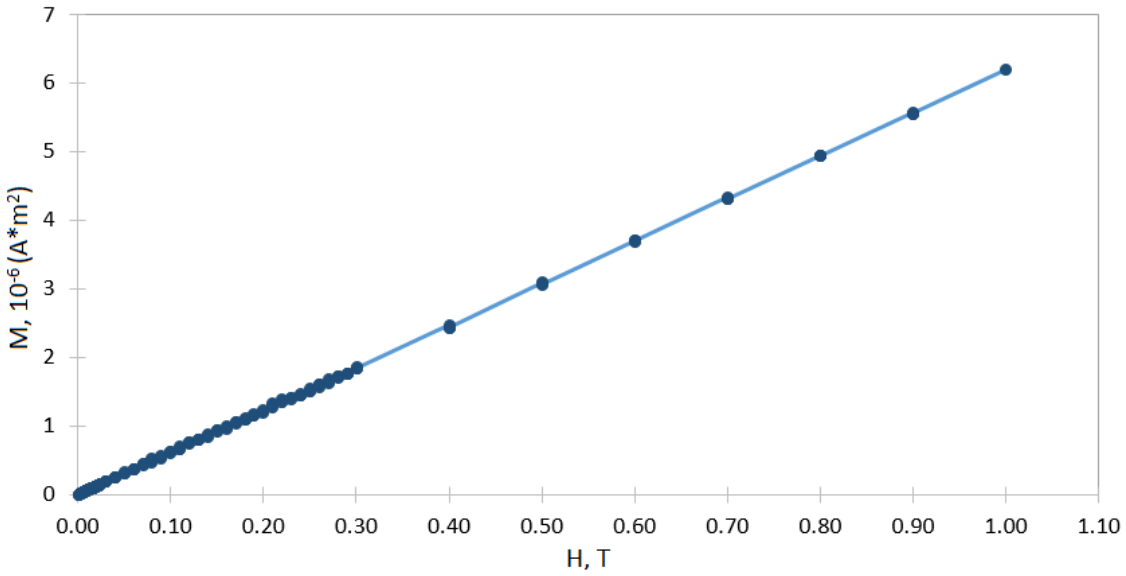

Figure 1. Field dependence of magnetization for paramagnetic platinum sample at constant temperature T = 298 K.

2.2 Paramagnetism

Paramagnets are magnetized in the direction of an external magnetic field, thus having a positive magnetic susceptibility. This is a non-cooperative magnetism, which arises from the presence of spontaneous magnetic moments in ions. Paramagnetism is observed in the case when the concentration of magnetic atoms or ions in the medium is relatively small and magnetic moments are separated from each other in a distance sufficient to regard them as noninteracting. On the one hand, the magnetic moments experience disorienting effect of thermal motion. The energy of such motion is kT. On the other hand, there is an ordering action of the external magnetic field. Atoms (molecules or ions) of the paramagnet have their own magnetic moments, which, under the action of external fields, are oriented along the field and, therefore, create a resultant field that exceeds the external field. In the absence of an external magnetic field, the paramagnet is not magnetized: intrinsic magnetic moments are oriented randomly due to the thermal motion of the atoms. Ideal paramagnet is characterized by susceptibility $\chi \approx 10^{-5}$ which varies inversely with the temperature T:

$$\chi = C\frac{B}{T}, \tag{3}$$

where B is magnetic flux and C is a Curie constant [9, 11, 12].

2.3 Ferromagnetism

Ferromagnetism is a cooperative type of magnetism, which can be explained by establishing collinear long-range order of all magnetic moments in the system at temperatures below the Curie point T_C. Therefore, even in the absence of the external field, a noticable magnetization exist, a so-called spontaneous magnetization. Ferromagnets are substances with strong magnetic properties. The reason for such strong properties is that the magnetic moments of the atoms are oriented in parallel, which leads to large magnetization called spontaneous magnetization. The ferromagnets behave as paramagnets above T_C. However, not only specific magnetic properties are observed below T_C, but also there are features in the behavior of nonmagnetic physical properties. Such anomalies reach a maximum near T_C. In the ideal ferromagnets, all ions have identical spontaneous magnetic moments and they occupy identical crystallographic positions. The ferromagnetism is an example of magnetism, in which the external field plays the role that makes it possible to reveal the existence of microscopic ordering at the macroscopic level [12].

The magnetic susceptibility of ferromagnets can reach $10^4 - 10^5$. The magnetization increase in the external magnetic field, grow with its magnitude nonlinearly. Magnetization can reach magnetic saturation in fields which are about $1 - 100G$. The value of magnetization depends on the "magnetic history" of the sample, which leads to the magnetic hysteresis in $M(H)$ [9].

2.3.1 Magnetic hysteresis

Magnetic hysteresis is a phenomenon where the magnetization vector depends not only on the applied external field, but also on the history of the given sample (See Fig.2). Magnetic hysteresis is usually manifested in ferromagnets, i.e., Fe, Co, Ni and alloys based on them.

The phenomenon of magnetic hysteresis is observed not only when the external field changes its sign. Also the so-called hysteresis of magnetic rotation occurs during magnetic flux rotation. It corresponds to a lag in the change of the direction of the magnetization with a change in direction of the field. The theory of the hysteresis phenomenon takes into account the specific magnetic domain structure of the sample and its changes

during magnetization and remagnetization. These changes are due to displacement of domain walls and the growth of some domains, as well as rotation of the magnetization vector in domains under the action of the external magnetic field. Anything that delays these processes and facilitates the entry of magnets into metastable states can cause the magnetic hysteresis [13, 14].

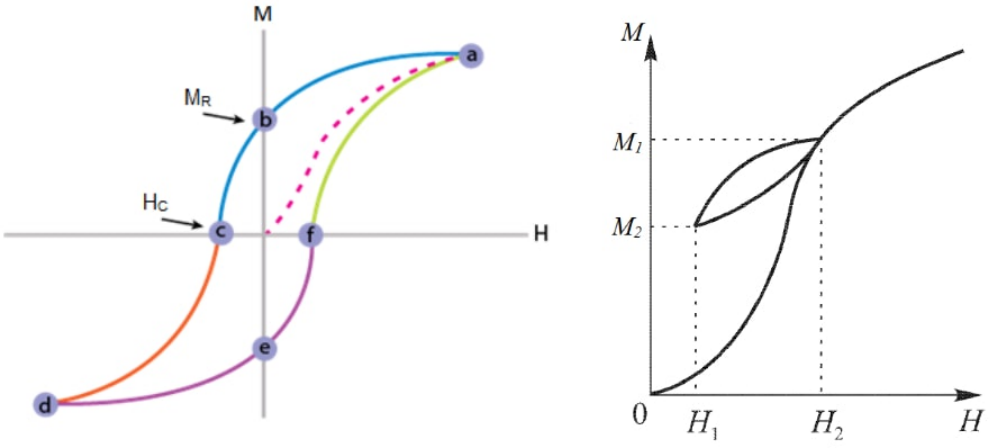

Figure 2. Magnetic hysteresis loop of ferromagnetic materials (on the left) and partial hysteresis loop (on the right). It is worth to emphasize that residual magnetization (M_R), coercive force (H_C) and magnetic susceptibility (χ) strongly depend on the nature of the sample processing [15].

Increasing the magnetic field from zero, at some point the magnetization saturation will be reached (dash-dot line in Fig. 2). However, if one reverses the magnetic field back to zero, the magnetization will decrease via the a-b curve. The lag of the magnetization from the field is an important characteristic of the magnetic substance. This determines irreversible energy losses during the magnetization reversal. The value M_R is called the residual magnetization of the substance. If one varies the field in the opposite direction, the magnetization will reach zero at field H_C, called coercive force. Further field increasing leads to an increase in the negative magnetization and saturation. If the field in the forward and backward directions is changed in some small interval between H_1 and H_2, a partial hysteresis will be obtained (See Fig. 2) [11, 15].

2.4 Antiferromagnetism

In antiferromagnetism, the neighboring spins (two sublattices) in the magnet are directed in opposite directions and compensate each other. It leads to the absence of spontaneous magnetization and strong magnetism. Therefore, they are classified as weak magnets and their susceptibility have the same order of magnitude as for paramagnets ($10^{-5} - 10^{-4}$). Neighbouring spins in antiferromagnets are oriented antiparallel due to strong interaction, so their stable ordering is preserved up to high temperatures. With such ordering, the strong interaction prevents moment orientation along the applied field. The effect is related to spin structure properties of the antiferromagnet near the interface, namely, with its domain structure, stabilized by nonmagnetic defects. The latter is responsible for the formation of domains in antiferromagnets and the domains are distributed so that the number of spins in its two sublattices is not the same [12, 16].

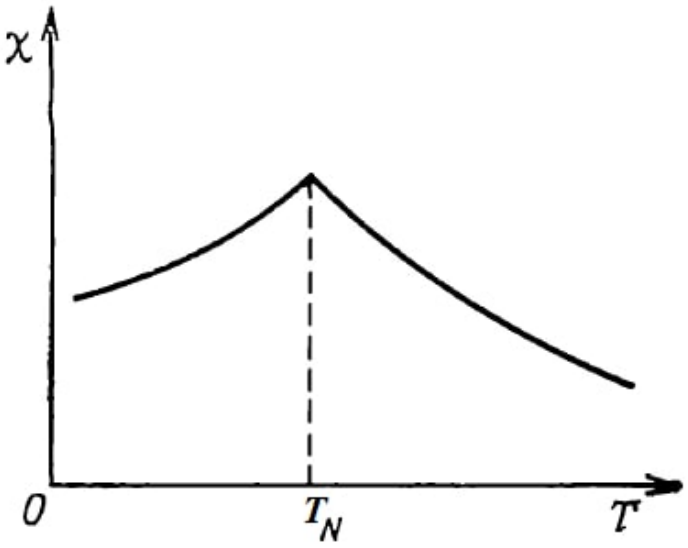

Figure 3. Magnetic susceptibility vs temperature dependence of the antiferromagnets. T_N is the Neel temperature above which the antiferromagnet loses its specific magnetic properties and changes into the paramagnetic state [17].

From the thermodynamic point of view, the Neel temperature T_N is similar to the ferromagnetic Curie point. The ordering gradually breaks and the susceptibility increases with the rise of temperature. Above the T_N, the order is replaced by the disorder and the susceptibility decreases. This is an important characteristic feature of the antiferromagnetism [15].

3 Heusler alloys

Heusler alloys are ternary intermetallic compounds with face-centered cubic crystal structure. The stoichiometric ratio is XYZ ("Half-Heusler" alloys) or X2YZ ("Full-Heusler" alloys), where X and Y are transition metals, and Z is the elements of III-V groups (See Fig. 4) [18, 19].

Heusler alloys with XYZ composition are considered as the third class of materials for possible applications in spintronics along with semiconductors and magnetic oxides, due to their semi-metallic properties, high T_c and tunable electronic structure. Atoms distribution and degree of structural order influence on the electronic structure and, therefore, physical properties of the Heusler alloys. The magnetic properties of the Heusler alloys strongly depend on the local geometry and chemical composition of the alloys [1]. They have ferromagnetic properties due to double exchange mechanism between neighboring ions [20, 21].

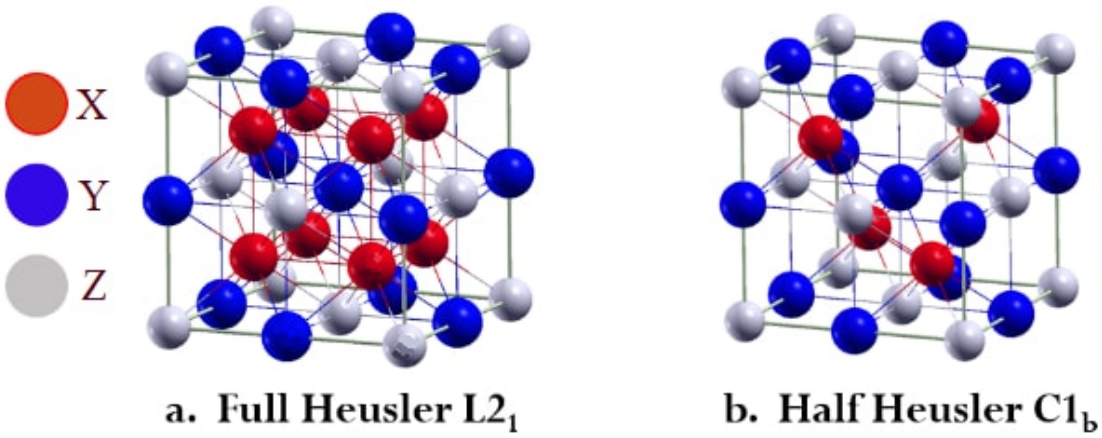

Figure 4. Structure of the Heusler alloys. For Full Heusler alloys (e. g., Co_2MnSi), two sublattices are occupied by X-atoms ($L21$ structure). For the Semi-Heusler alloys, one face cubic centered sublattice remains unoccupied ($C1b$ structure).

4 Phase transitions

4.1 First and second order phase transitions

Transitions from one phase to another with the change in the state parameters are called phase transitions. The process is the result of changes in external conditions such as temperature, pressure, magnetic and electric fields. The value of temperature, pressure, or some other physical parameters, at which phase transitions occur is called transition point.

During the first order phase transition (FOPT), such thermodynamic characteristics of substance as density and components concentration change abruptly. The parameters expressed by the first derivatives of the Gibbs free energy (G) with respect to pressure (p), temperature (T), and magnetic field (H) vary abruptly (See Eq. 4).

$$S(T,H,p) = -\left(\frac{\partial G}{\partial T}\right)_{H,p} M(T,H,p) = -\left(\frac{\partial G}{\partial H}\right)_{T,p} V(T,H,p) = \left(\frac{\partial G}{\partial p}\right)_{T,H} \quad (4)$$

In this case a certain amount of heat per unit of mass, called the phase transition heat, is released or absorbed in unit of mass. The FOPT is characterized by presence of hysteresis phenomenon (e.g., overheating or subcooling of one of the phases) during which the nucleation of another phase occurs. The same phase can exist on both sides of the transition point on the phase diagram. At the point of the FOPT, the Gibbs free energy as a function of the state parameters is continuous, and both phases can co-exist for arbitrarily long time (for example, the coexistence of a liquid and its vapour). First order phase transitions are widespread phenomena in nature. They include evaporation and condensation, melting and solidification, sublimation and condensation, most polymorphic transformations, some structural transitions in solids, for example, martensitic and inverse martensitic transitions, which will be discussed later. In pure superconductors a sufficiently strong magnetic field causes FOPT from the superconducting state to the normal state [22, 23].

In case of second order phase transition (SOPT), the G value and the first derivatives of G with respect to T, p and H vary continuously, whereas the second derivatives, heat capacity, compressibility and thermal expansion are noncontinuous. The heat is not released

or absorbed, hysteresis and metastable states are absent. The SOPT, observed with the temperature change, include transitions from the paramagnetic (disordered) state to the magnetically ordered (ferro- and ferrimagnetic in the T_c and antiferromagnetic at Neel temperature) with the appearance of the spontaneous magnetization, as well as, dielectric - ferroelectric transitions with the appearance of spontaneous polarization [24].

4.2 Magnetic phase transitions

For all magnetically ordered substances there is one common feature: a correlated disappearance of microscopic magnetic moments at T_c. This phenomenon is associated with destruction of the magnetic order and represents the magnetic phase transition of a order-disorder type. As a parameter, one can consider the average thermodynamic value of the magnetic moment of an atom in a crystal. Therefore, the magnetic order parameter has nonzero value in the ordered phase and zero in the unordered phase. The reason for spontaneous formation of the magnetic order is the existence of strong interatomic interaction, depending on the relative orientation of the nuclear spins. With increasing temperature, the competition between the ordering effect and the thermal motion of the magnetic moments leads to a decrease in the magnetic order parameter. Long-range magnetic order disappears when the temperature reaches value at which the thermal energy and the interatomic interactions become comparable. Transitions associated with disordering differ in the nature of the change in the magnetic order parameter. Smooth and abrupt change of the parameter is possible when the temperature approaches the characteristic temperatures. In the first case, the magnetic order parameter can take any values close to zero when T is near to T_c from the low-temperature region. In the second case, infinitesimally small values of the magnetic order parameter during the transition are not realized. These describe second and first order phase transitions. The latter are characterized by an abrupt change not only in the magnetic order parameter, but also in the volume of the unit cell. Along with order-disorder transitions in magnetically ordered substances, transitions associated with a change in the type of magnetic ordering are also observed. In this case, the order parameter can remain finite before and after the transformation [25–27].

4.3 Martensitic transitions

Martensitic transition is the diffusionless first order phase transition between two phases: austenitic (AP) and martensitic (MP). Austenite is a high-temperature phase with face-centered cubic lattice $L21$ and martensite is a low-temperature phase with a body-centered cubic lattice $L10$. The structure of both phases is shown in Fig. 5. It is structural transformation, in which the change in the mutual arrangement of atoms (molecules) occur as a result of displacements of neighboring atoms in distances smaller than the interatomic distances. The martensitic transition temperature is related to its electronic structure and is defined by valence electron concentration (e/a) (See Fig. 6b) [28]. Reorganization of the crystal lattice usually lead to deformation of its unit cell and to a decrease of the symmetry degree. Final phase of the martensitic transition can be regarded as the homogeneously deformed initial phase. The magnitude of the deformation is small and, therefore, the energy barrier, which prevents the homogeneous transition from the initial phase to the final one, is low. The martensitic transformation temperature depends on the chemical composition and the external magnetic field value [29].

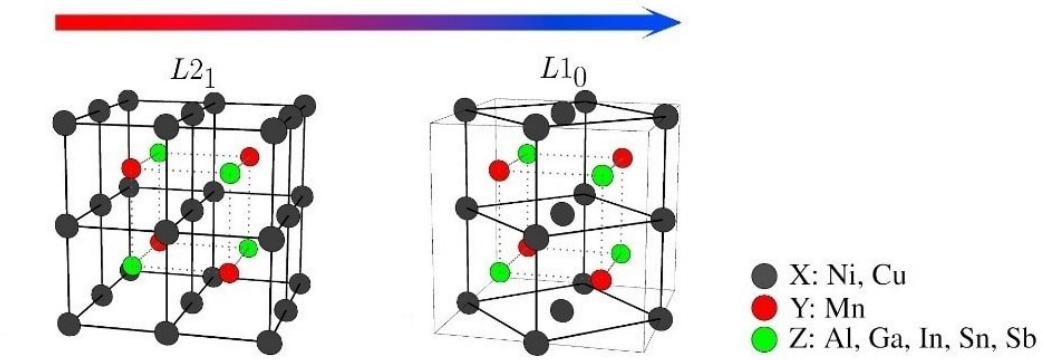

Figure 5. Crystal structure of the austenitic ($L21$) and martensitic ($L10$) phases [30].

Direct martensitic transformation occurs by nucleation and subsequent growth of the martensitic phase regions, so that during the martensitic transition the medium is a mixture of two phases. M_s/M_f and A_s/A_f are "start" and "finish" temperatures of direct (M) and reverse (A) transitions (See Fig. 6a). At M_s temperature the martensitic phase nucleation begin, MP/AP ratio is close to zero, whereas at M_f the MP/AP ratio is approximately 1. The speed of transition is comparable with the sound speed in materials ($\approx$ 1000 m/s). The martensitic transitions can be thermoelastic, that has relatively small volume change and a narrow hysteresis; and non-thermoelastic, characterized by big volume change and a wide hysteresis. However, it is problematic to distinguish the type

of martensitic transition because they are both reversible and the difference in hysteresis width and volume change sometimes is poorly visible. In addition, there is magnetostructural transitions that lead to simultaneous change in the structure and magnetic state of the material [31, 32].

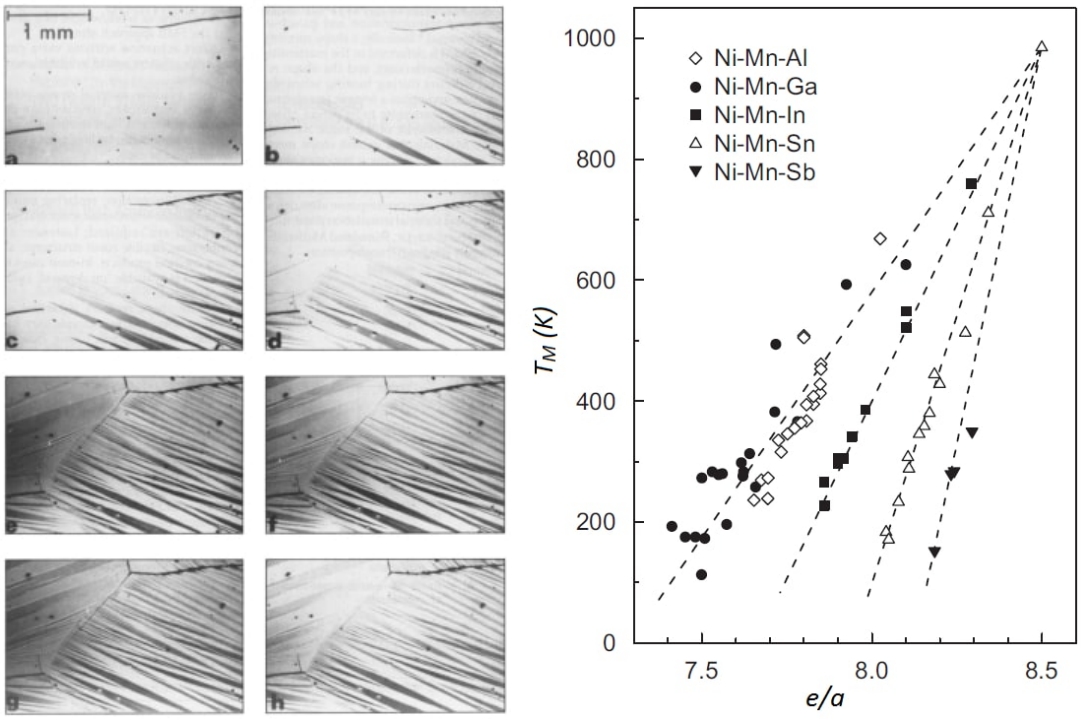

(a) (b)

Figure 6. (a) Formation of the martensitic phases during the martensitic transition (MT). The upper left picture corresponds to the start temperature of the MT and the lower right one to the final temperature [33]. (b) The martensitic transition temperature dependence of the valence electron concentration [28].

The martensitic transformation has number of features:

- various kinds of defects exist in structure of martensitic phase after the MT,
- the transformation can be determined by the appearance of irregularities on the polished flat surface of the sample,
- transition temperatures strongly depend on the chemical composition of the sample and external conditions (e.g., magnetic field),
- the martensitic transition can be observed at temperatures above and below the Curie temperature [34].

Shape memory effect is one of the most decisive Heusler alloy's effects. The effect is directly related to the martensitic transformations and can be regarded as possibility of deformed sample to return its shape during heating. The restoration value can reach up to 10% of original shape. The deformation does not occur when the sample is cooled from the AP (A_f) to the MP (M_f). However, if one deforms the sample in the MP it will remain in the deformed state until heating. The heating causes the shape restoration during the inverse martensitic transition, where the start and finish temperatures are A_s and A_f, respectively. Further form changes can be achieved only by external force deforming in the MP state. This a so-called one way shape memory, cooling back from AP to MP does not induce any changes [35].

However, under certain conditions shape restoration can be achieved during cooling. This is a so called two-way shape memory effect. In this case, after shape restoration during heating, the cooling will cause the deformation. For instance, earlier contracted conventional spring, will extend during heating and contract during cooling, and the process can continue infinitely [33, 36].

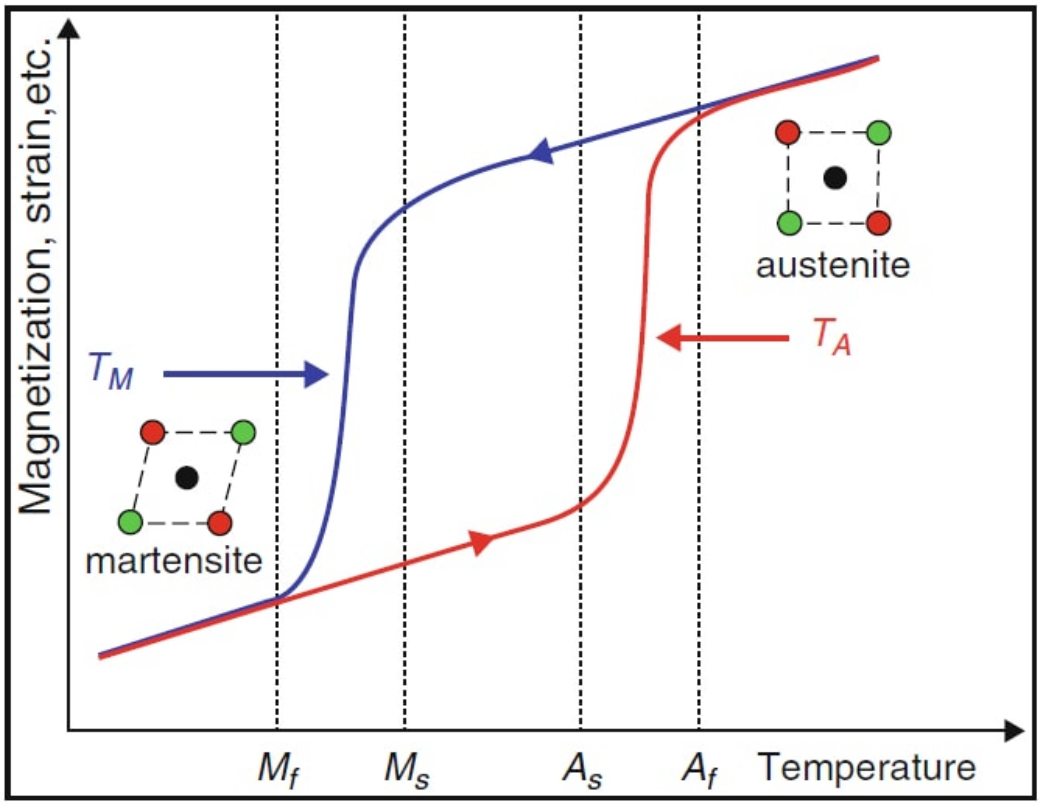

Figure 7. Schematic representation of the martensitic transition (blue line), reverse martensitic transition (red line), austenitic and martensitic phases. T_M and T_A are temperatures of direct and inverse martensitic transitions, correspondingly [34].

5 Magnetocaloric effect

The magnetocaloric effect (MCE) is the temperature change of a material during magnetization or remagnetization in external magnetic field under adiabatic conditions (i.e. in the absence of heat exchange with the surrounding medium). Emil Gabriel Warburg observed this effect in 1881 when the sample of iron was remagnetized. For long time the MCE had no practical application, but in 1926 Peter Debye and William Giauque proposed a method to obtain super low temperatures by adiabatical demagnetization of paramagnetic salts. Magnetocaloric effect investigation had been hampered by the fact that ferromagnetic materials with the T_c near the room temperature was not known until the discovery of the ferromagnetism in gadolinium in 1935. In 1997, Pecharsky V. and Gschneidner K. discovered the so-called giant magnetocaloric effect in the $Gd_5Si_2Ge_2$ compound [37]. The value exceeded the values of all previously known ferromagnetic alloys, which contributed to the growth of the number of scientific articles [38]. The magnetocaloric effect arises as a result of the redistribution of the internal energy of the magnetic substance between the system of magnetic moments of its atoms and the crystal lattice. The maximum value of the MCE is reached at temperatures of the magnetic phase transition, for example, in the region of the Curie temperature of ferromagnets. Applying the magnetic field causes heating of the ferromagnet, and the removal of the field leads to cooling. The adiabaticity of the process is achieved by a rapid change in the magnetic field. The variation in the thermal state of the sample manifests itself as the change in its temperature and the magnetic part of the sample entropy. The change is characterized by two values: adiabatic change of the temperature (ΔT) and isothermal change of the magnetic part of the entropy (ΔS_m). In the case of the solid, the lattice part of entropy ΔS_{lat}, which characterizes the thermal state of the lattice and the motion of its atoms, can be associated with the crystal lattice. The magnetic part of the entropy S_m characterizes degree of ordering of the magnetic subsystem. The total entropy of the material is the sum of the magnetic, lattice and electron contributions to the entropy [23].

$$S(H,T) = S_m(H,T) + S_{lat}(H,T) + S_e(H,T). \tag{5}$$

All three contributions depend on the temperature and magnetic field strength and can not be clearly separated. When the material is placed in a magnetic field, the degree of its magnetic ordering will change. This will cause a change in the magnetic part of the entropy on the value ΔS_m. If the process is adiabatic, then the change in the magnetic part of the entropy will cause a corresponding changes in the lattice part: $\Delta S_{lat} = -\Delta S_m$ [39].

Thus, the MCE arises from the changes in the ordering of the magnetic subsystem of the material and the interaction between the crystal lattice and the magnetic subsystem. The energy spent in disorientation of the magnetic moments is transformed into energy of lattice vibrations which cause change in the temperature. Figure 8 shows the dependence of the total entropy of the material on the temperature in the presence and absence of the magnetic field. The point A in Fig. 8 displays the entropy of the sample at temperature T_1 in the absence of magnetic field. However, if the sample is placed in the magnetic field under adiabatic conditions, then its transition from thermodynamic equilibrium A to B will occur. In this case, the sample temperature will change on the value $\Delta T = T_2 - T_1$. However, if the process would be isothermal, then the sample goes from state A to state C. In this transition, total energy changes on the value $\Delta S_m = S_2 - S_1$ [40].

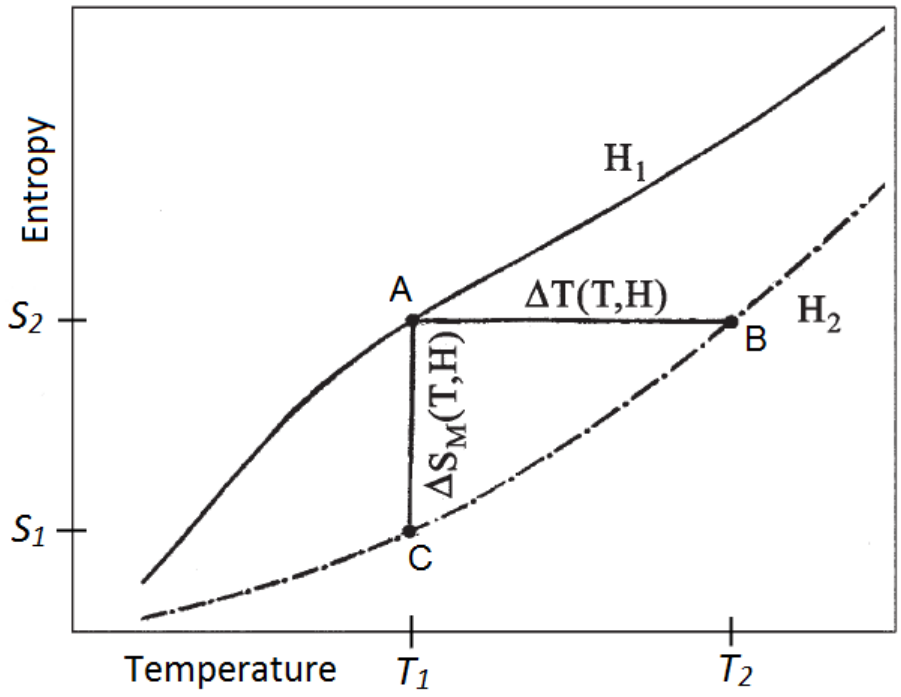

Figure 8. Total entropy as a function of temperature in zero (H_1) and nonzero (H_2) magnetic fields [23].

The values, characterizing the MCE, are determined either by a direct method (measuring the temperature change of the sample, magnetized under adiabatic conditions) or can be calculated indirectly on the basis of magnetization or heat capacity measurements. Knowing the magnetization values, one can calculate the ΔS_m by using the Maxwell relation:

$$\left(\frac{\partial S}{\partial H}\right)_{T,p} = \left(\frac{\partial M}{\partial T}\right)_{H,p} \tag{6}$$

The maximum values of the MCE are achieved in the region of first order magnetic phase transitions, especially in the case when the magnetic transition is accompanied by the structural transition [30].

6 Exchange bias

Exchange bias phenomenon is known as a shift of the magnetic hysteresis loop of materials when cooled in presence of the external magnetic field. The shift (H_E) is due to material heterogeneity that is attributed to antiferromagnetic (AFM) coupling of ferromagnetic (FM) AP and MP phases. The value of exchange bias (EB) depends on magnetic moments orientation of FM phase and one of sublattices of the AFM phase. The system must be cooled down below T_N in the presence of magnetic field that is larger than the saturation field of FM phase. At temperatures close or above the T_N, the phenomenon disappears due to the absence of the AFM phase which cause anisotropy of the system. Moments of the AFM phase sublattice coincide with the FM phase moments which create strong exchange coupling (See point 1 in Fig. 9). The opposite external field force to change the moment direction of the FM phase but the FM/AFM coupling tends to pin the moment direction of the FM in the original direction, resulting in hysteresis shift H_E (See point 2 in Fig. 9 and Fig. 10). Therefore, a strong opposite field is needed to overcome the pinning (See point 3 in Fig. 9). The scope of this effect vary from spin valves and reading heads to nonvolatile memory. The EB effect was observed in many different systems such as small particles, thin films, FM films on AFM single crystals and inhomogeneous materials [5, 34, 41, 42].

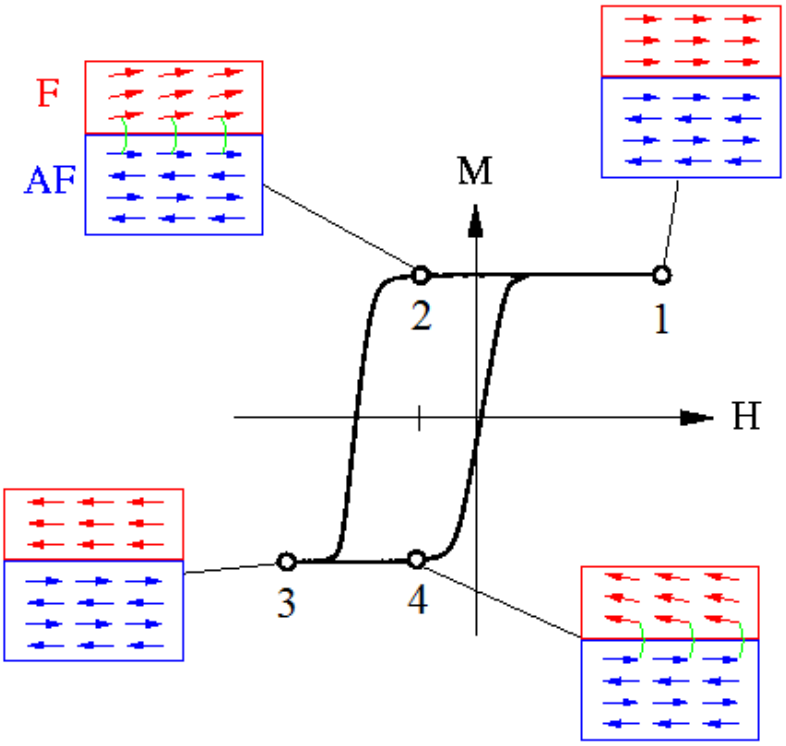

Figure 9. Schematic representation of FM/AFM coupling and the hysteresis shift [42].

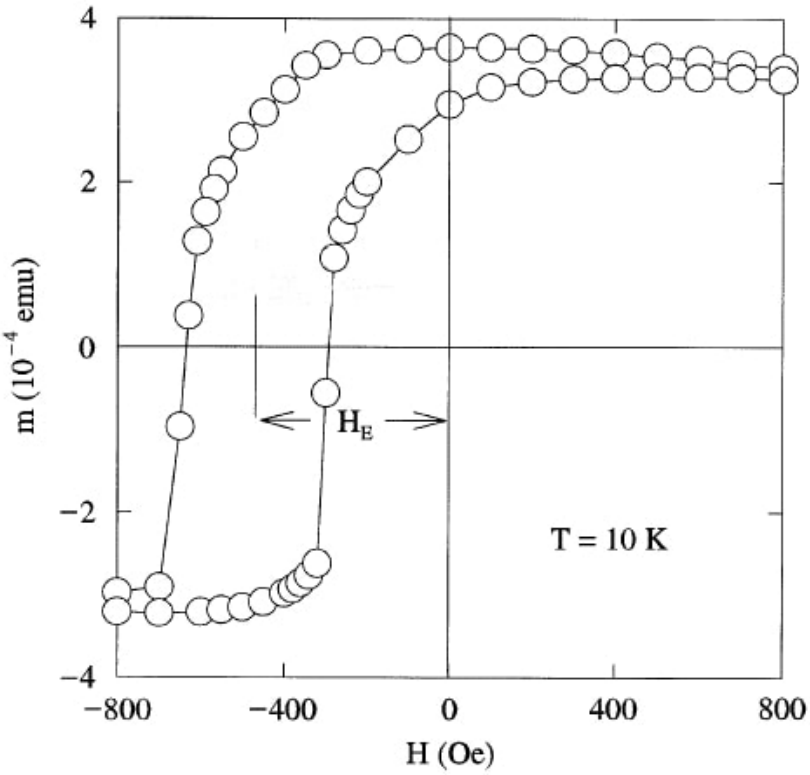

Figure 10. Representation of horizontal magnetization shift in the hysteresis loop of a FeF_2/Fe bilayer [5].

7 Determination of magnetic entropy change

Three essential parameters can be proposed for MCE value estimation: $\Delta S_m, \Delta T_{ad}$ and RC (See Formulas 7, 8 and 9) In order to calculate it, temperature ($M(T)$) or field dependencies ($M(H)$) of the magnetization is needed. The ΔT_{ad} of the sample can be directly measured without any calculation. The RC value is the energy transferred between hot and cold states. Magnetocaloric materials can be divided in two classes: Some of them experience first order phase transition, and other undergo the second order phase transition. It is worth to notice that MCE value depends on the phase transition order. For the case of SOPT (ferro-paramagnetic transition near T_c), there is not coexistence of different phases and the magnetization fall down to zero value after phase transition temperature. Temperature and magnetic hysteresis are absent in such transition. Opposite situation is observed in case of FOPT: The material experience the coexistence of different phases and exhibit abrupt change of magnetization, associated with magneto-structural phase transition. One needs to degauss the sample after each temperature point during $M(H)$ measurements in order to keep the sample in one phase [43]. Generally, FOPT materials exhibit large ΔS_m in comparison with SOPT materials. However, the first ones have more narrow peaks over the temperature range [4].

$$\Delta S_m = \mu_0 \int_0^H \left(\frac{\partial M}{\partial T}\right)_H dH \tag{7}$$

$$\Delta T_{ad} = \mu_0 \int_0^H \frac{T}{C_H} \left(\frac{\partial M}{\partial T}\right)_H dH \tag{8}$$

$$RC(\Delta H) = \int_{T_{cold}}^{T_{hot}} \Delta S_m(T, \Delta H)\, dT \tag{9}$$

8 S700X SQUID magnetometer

A superconducting quantum interference device (SQUID) magnetometer is device for measuring the static magnetic properties (magnetic moment versus temperature or magnetic field) of a wide range of objects: from strongly magnetic ferro- and ferrimagnets to spin glasses, multilayer films and nanostructures. In recent decades, among the various methods of magnetic measurements, the SQUID magnetometry has been developed and improved intensively due to their phenomenal sensitivity (in comparison with other methods). The sensitivity reaches 10^{-6} flux quanta Φ_0 variations in magnetic field that makes it possible to measure samples containing small amount of magnetic impurities and, that is not less important, in low magnetic field strength. The above-mentioned advantage has given opportunity to effectively use the SQUID in various fields of science: biomedicine, geophysics, solid-state physics, etc. The S700X SQUID Magnetometer, which was used in the measurements, is shown in Fig. 11. The sample temperature can vary from 1.6 K to 400 K. The magnetic field, generated by superconducting coils, can create a 7 T magnetic field. The SQUID has several modes of operation. However, only one mode was used in the measurement (extraction magnetometry), the essence of which is to measure the total magnetic moment by moving the sample through a set of pick-up coils (a scan length can be varied from 2 to 120 mm, however, 4 cm length was used in measurements). All magnetic measurements are performed exclusively in the short-circuit mode of the superconducting solenoid. The magnetic flux in the solenoid circuit is quantized, and the magnitude of the magnetic field assumes strictly fixed values (DC measurements) that is essential for materials which exhibit magnetic hysteresis. This is a significant advantage of the system, because the coils register a constant magnetic flux so that it is not needed to move the sample with high speed through the pick-up coils.

Figure 11. Two main components of the SQUID magnetometer: cryostat (on the left) and rack (on the right).

8.1 Operation principle

SQUID magnetometer is a sensitive device for converting magnetic flux into electrical signal of DC/AC current, the action of which is based on the phenomenon of magnetic flux quantization in a superconducting ring with Josephson junctions included in it.

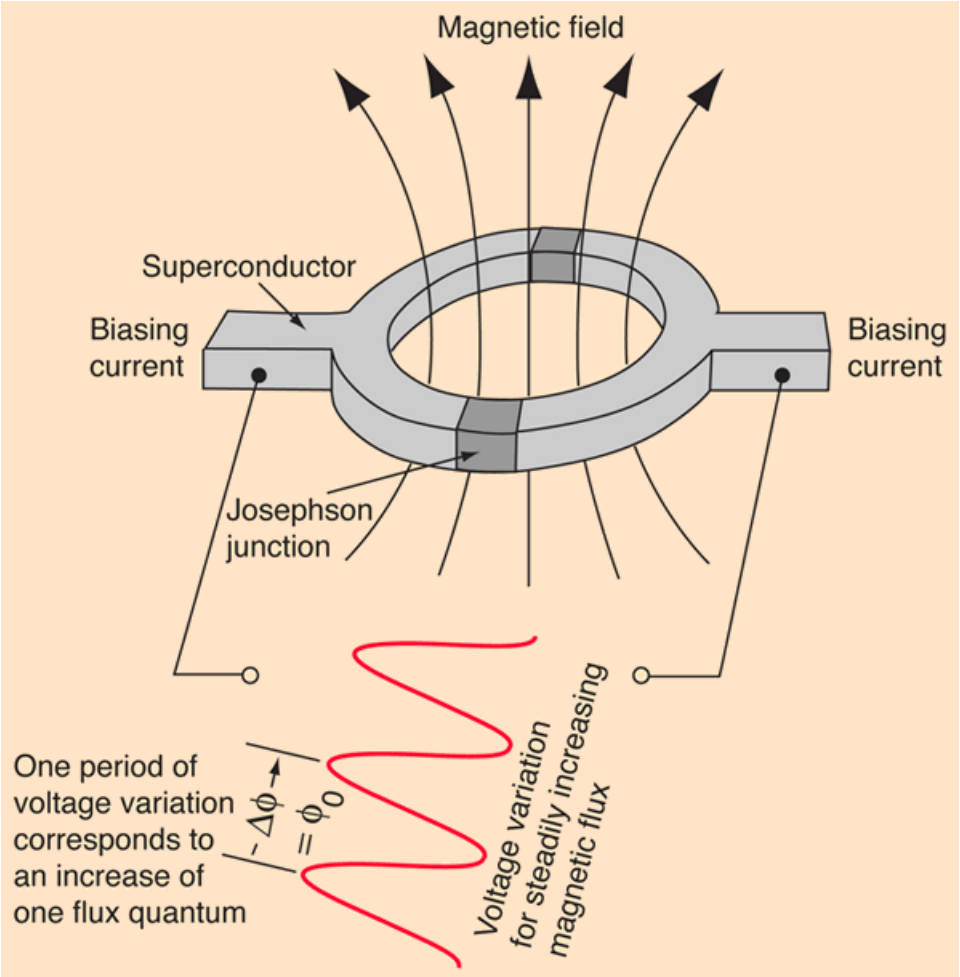

Figure 12. Illustration describing the Josephson effect with two superconducting regions and two Josephson junctions.

The simplest quantum magnetometer (SQUID) is a superconducting ring with two Josephson tunnel junctions. We know that electrons possess wave properties. The electron wave is divided into two, each of them passes through tunnel junction, and then both waves are converged together (See Fig. 12). In the absence of external field, both branches will be equivalent, and both waves will arrive without any phase difference. However, in the presence of magnetic field, circulating superconducting current will be induced in the circuit. This current will be subtracted from the constant external current in one of the contacts, and will be added in the second contact. Therefore, the two branches will have different currents, and phase difference will appear between the tunnel junctions. Electron waves, passing through the contacts, will interfere. The interference will manifest itself as a dependence of the SQUID current on the applied external magnetic field. The stepwise nature of the dependence makes it possible to distinguish individual flux quanta. In a way, this is analog of the optical effect with interference from two slits, but in this case currents interfere. [45, 46]

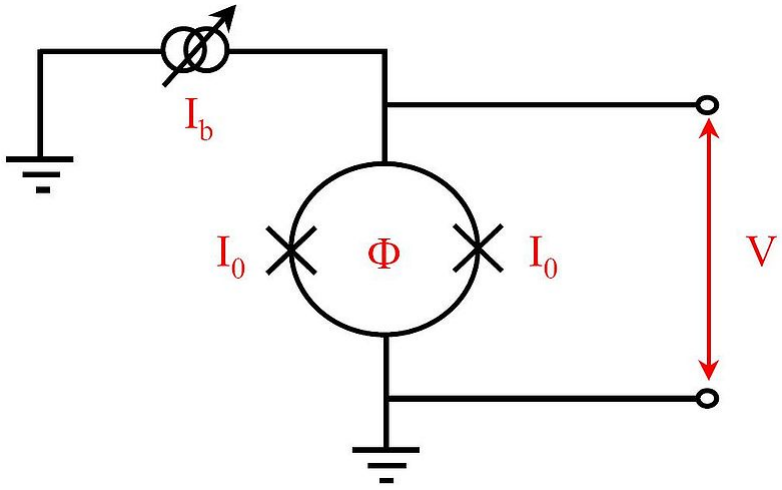

Figure 13. Circuit diagram of DC SQUID magnetometer, where I_b - external current through the superconducting ring, I_0 - critical current, Φ - magnetic flux applied to the circuit, V - voltage drop.

8.2 The recondensing cryostat system

The system features aluminium shell which contains a liquid helium reservoir with thermal radiation shield (the maximum volume is 49 L), a cryocoler and recondensing loop system to maintain the superconductivity of components. It is presented in Fig. 14. The system maintains constant low temperature of the working volume, that is needed to prevent the gas boil off. The Mu metal layer of outer shield prevents earth's magnetic field

penetration into the system. The cooling power is produced by the cryocooler, which is mounted on the top of the cryostat. In addition, the cryocooler liquefies closed helium gas loop (the recondensing loop).

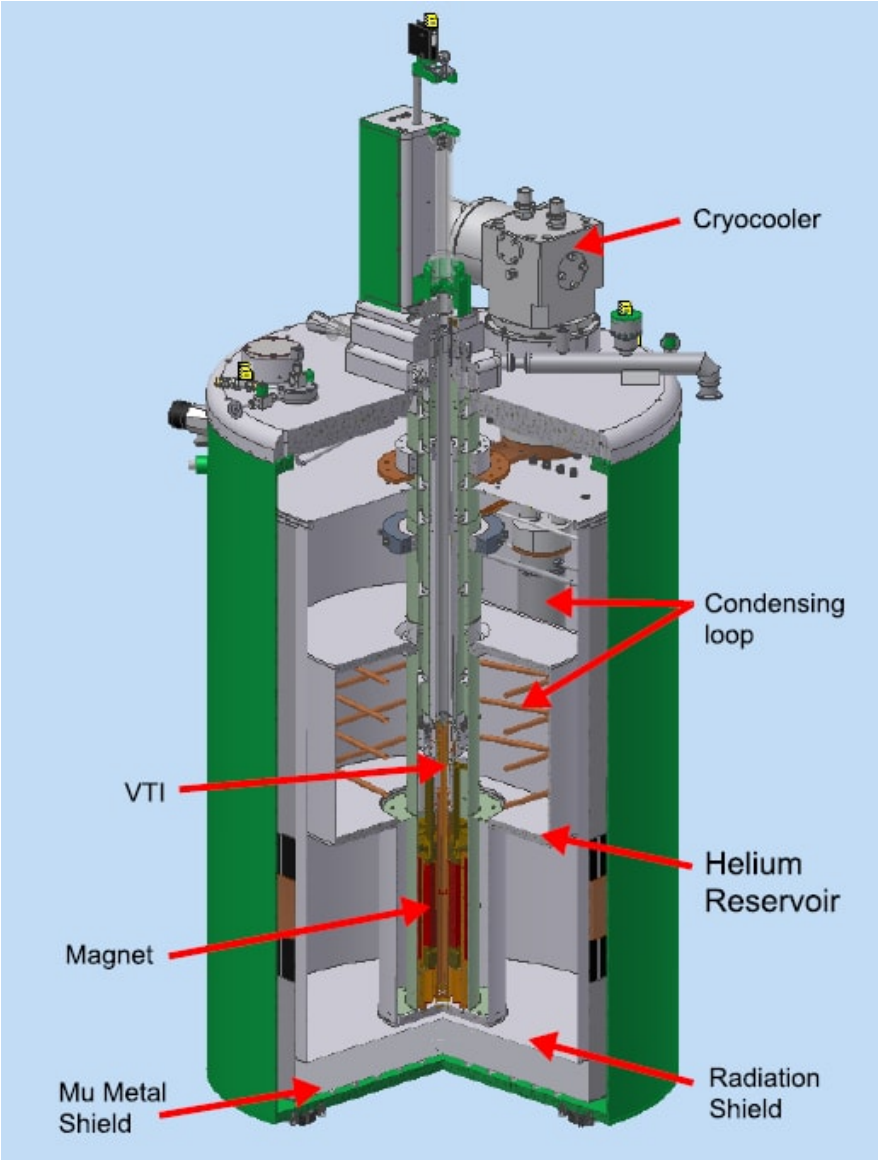

Figure 14. The internal structure of the recondensing cryostat system and magnetometer insert [44].

8.3 The magnetometer insert system

The main part of the system is variable temperature insert (VTI), which contains sample space, magnets and SQUID detector itself. Upper part of the VTI has airlock for sample mounting and stepper motor for vertical movement of a rod with sample on it.

8.4 The magnets

The bias field with high homogeneity and low drift can be increased up to 7 T. The diagram of magnets system is shown in Fig. 15. The system consists of two main parts: internal and external. The first part generates the bulk of magnetic field and the second part is utilized to maintain the homogeneity of the axial field and to minimize the stray field. In order to create the desired value of current in the winding of the inner coil, it is needed to heat the superconducting bridge into normal state. It can be achieved by switching on the heater, located on the superconducting wires. In normal state one can apply current and when it will stabilize, the heater is switched off and the superconductivity returns back. Then the power supply is switched off. It is not necessary to apply current to the system because the current can flow without any losses in the superconducting state.

8.5 The SQUID detector system

The detection of magnetic flux is performed by pick-up coils which are located in the center of magnetic system (See Fig. 16a). The pick-up coils are connected to input coil of the SQUID detection system forming a flux transformer. The flux change cause voltage change due to quantum effects. The SQUID detector is located above the magnets and shielded from environmental noise by niobium can. The SQUID measures relative changes in magnetic flux and, hence, it is necessary to move the sample through the coils. This cause a screening current to flow in the flux transformer circuit which opposes the resultant change in the flux through the pick-up coils. In SQUID electronics we can see a voltage directly proportional to the signal of SQUID detector.

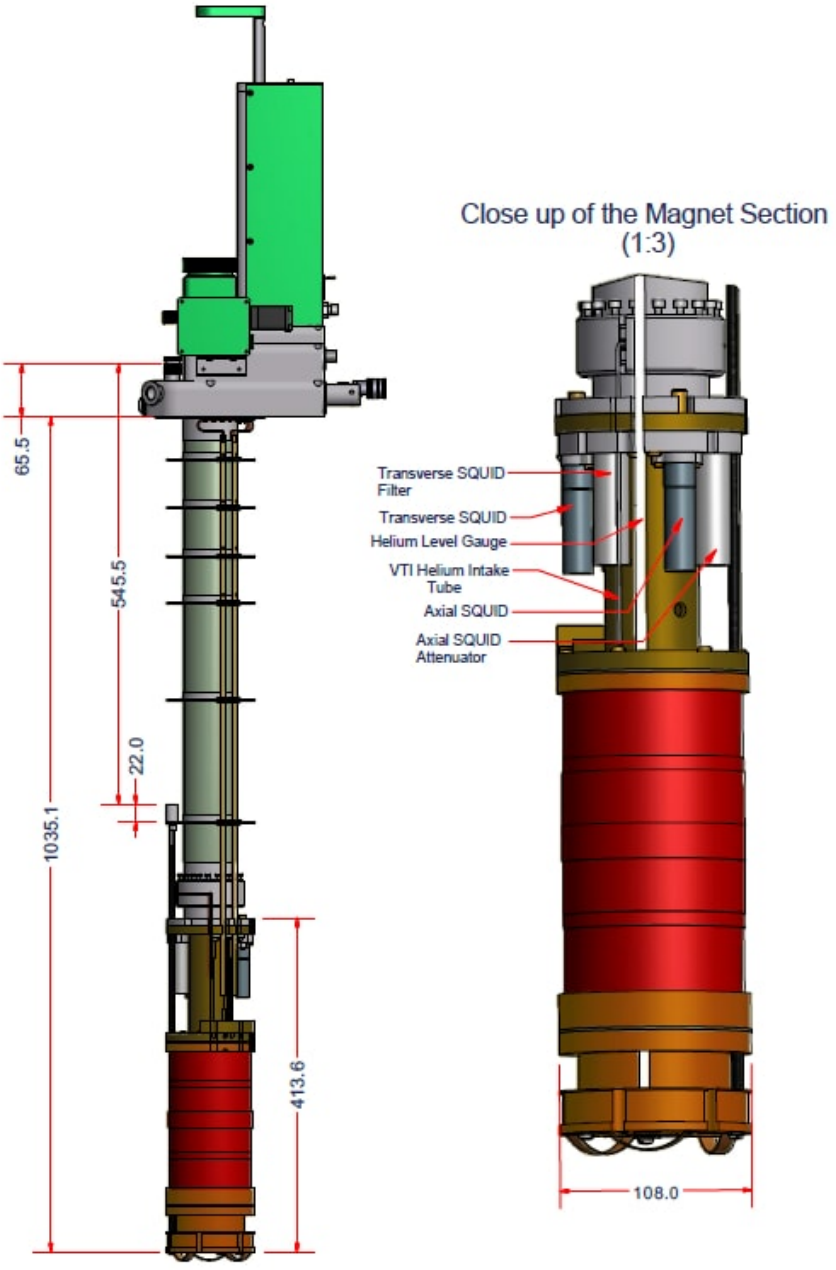

Figure 15. The structure of the magnetometer insert [44].

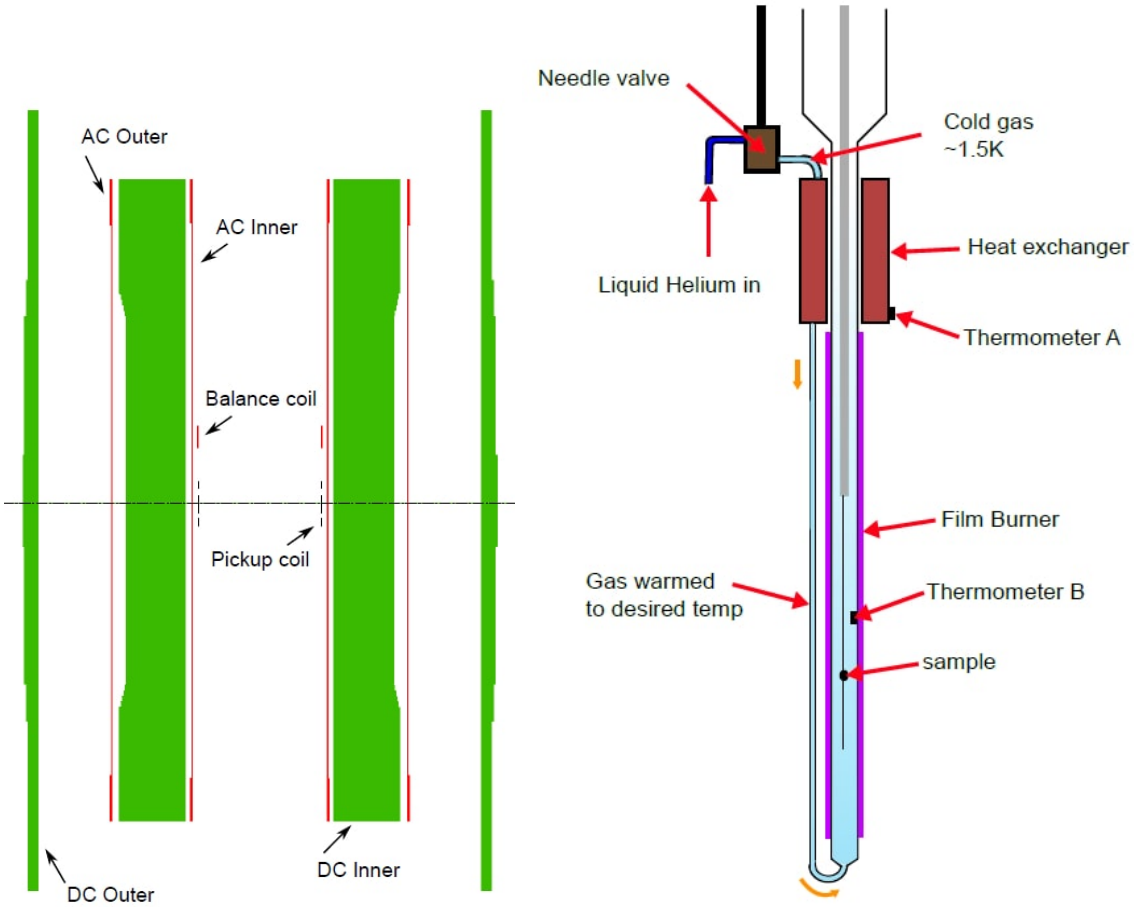

(a) (b)

Figure 16. Schematic cross-section of the magnet assembly showing the inner and the outer sections and representation of temperature control in the VTI [44].

The VTI can be roughly divided on two parts: the upper section is steel tube (19 mm in diameter) and the lower section is phosphor bronze tube (9 mm in diameter). The internal space of the tubes is thermally isolated from the cryostat (i.e. from liquid helium) by a vacuum interlayer. However, a needle valve that is located on the lower section, creates direct connection between the cryostat and the VTI (See Fig. 16b).

The liquid helium passes through the needle valve, which leads to a drop in pressure and, as a consequence, to temperature decrease. Further, we can increase the gas temperature by two heaters: heat exchanger and film burner (See Fig. 16b). The film burner is necessary for heating rate increasing. As can be seen from the figure 16b, the system has two thermometers: it is important to reach equilibrium between them before measurement (which is done automatically, but sometimes take too much time) [44].

8.6 The electronic rack

The electronic systems are housed in a standard width electronics rack (W 59.9 cm $\times$ H 174.0 cm $\times$ D 80.0 cm). The rack consists of:

LakeShore 218 monitors temperatures of some thermometers located inside the cryostat.

Temperature Controller monitors all thermometers and controls the temperature of the VTI heat exchanger.

Level gauge and DC SQUID interface measure the level of the liquid helium in the reservoir. The SQUID output can be monitored via a BNC connector and also displayed on the panel.

Stepper motor panel controls the sample position within the pick up coils. Front panel LEDs indicate that the motor is activated.

Data acquisition unit (DAQ) / Valve block indicator panel control all analogue and digital inputs and outputs to the system hardware except the magnet power supply and temperature controller. The red LED indicates power to the data acquisition unit and the green LED indicates that computer is properly connected. A schematic diagram of the helium circuit is light with red/green LEDs indicating which valves are closed/open, respectively.

Electronic filter unit houses the electronic filtering circuits for all electrical services connected to the insert, the power supplies for the VTI heaters and SQUID/magnet detection circuit.

Computer runs the S700X software and controls the various electronic systems.

Superconducting magnet power panel controls the current in the superconducting magnet.

Valve block module contains the electronically controlled valves that operate gas systems as well as a pressure gauge for the VTI.

9 Measurements

The sample is the polycrystal $Ni_{48.5}Co_{1.5}Mn_{35}In_{15}$ weighing 1.8 mg which was fabricated by conventional arc-melting method from 4N purity metals in argon atmosphere. In order to achieve homogeneity, the sample was annealed in high vacuum ($\approx 15 - 5$ torr) for 24 hours at 850 °C temperature [6].

Using teflon tape (PTFE), the sample was fixed to a copper wire (See Fig. 17) that was connected to the rod by which the sample is immersed in the VTI at a desired level.

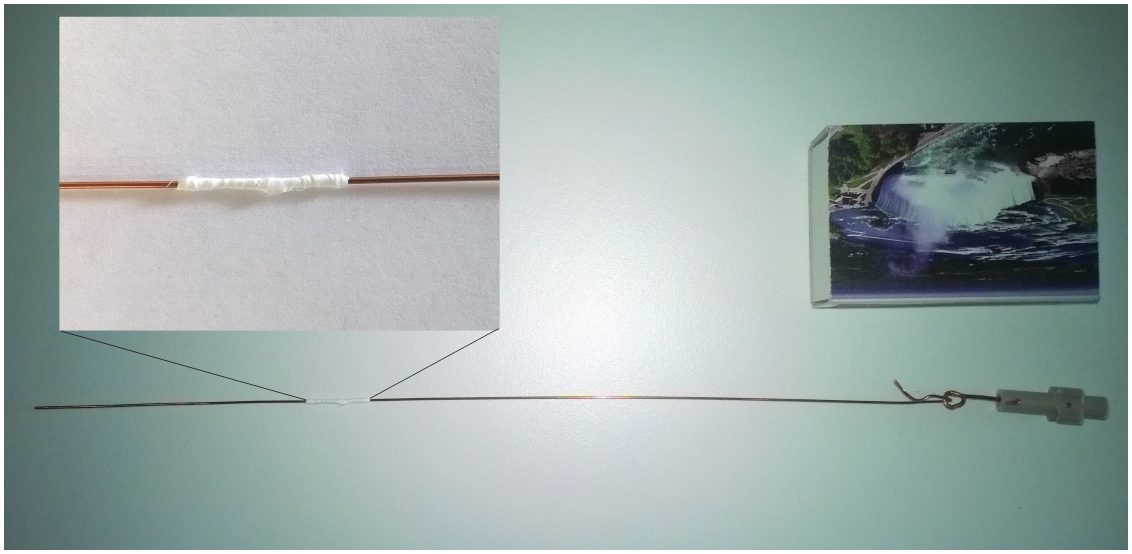

Figure 17. A copper wire with the sample attached on it by teflon tape.

Investigation of microstructure was performed by X-ray powder diffraction method using Bruker Advance D8 automatic diffractometer operating at 40 kV and 40 mA, in theta-theta configuration, equipped with secondary monochromator with Cu-Kα radiation (λ = 1.5418 Å).

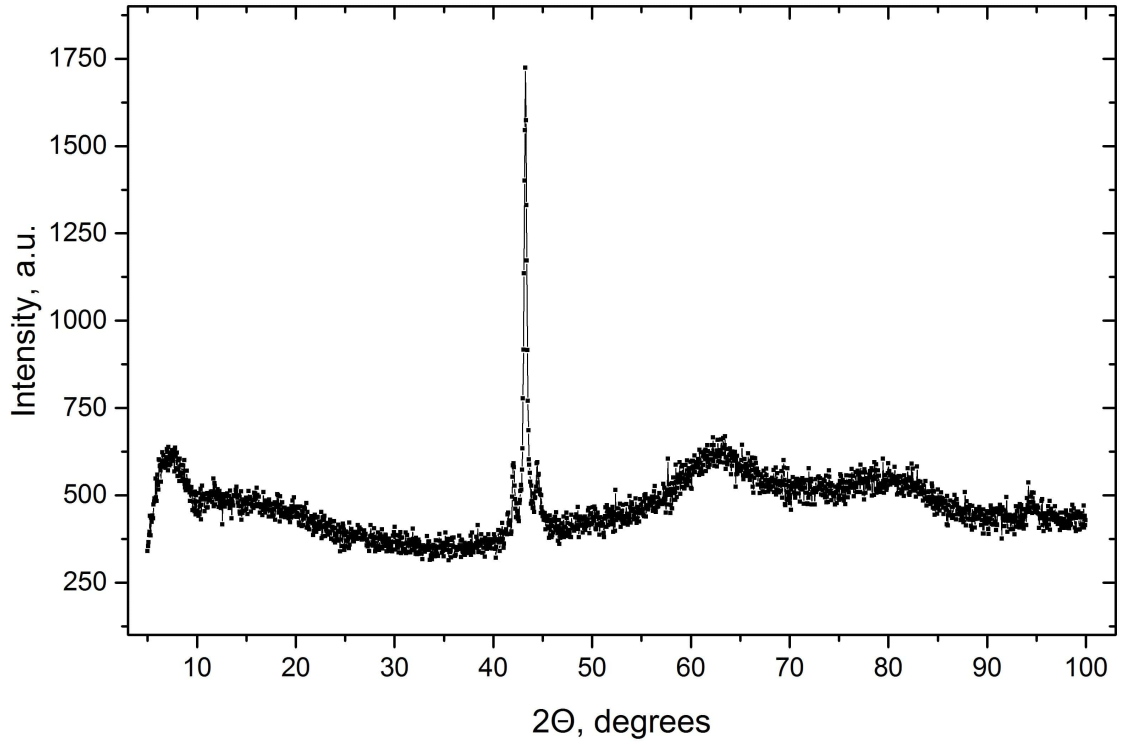

Figure 18. X-ray diffraction pattern measured at room temperature.

There are three distinct peaks, where the middle one is of the highest intensity. The rest is background coming from sample holder and parts of the setup. The peaks indicate that the sample is in single phase with well defined bode-centered cubic L10 type at T = 298 K [47].

First of all, temperature dependencies at two different fields (100 Oe and 5 T) were carried out with the SQUID magnetometer. Martensitic transition temperature (T_M), Curie point (T_C), blocking temperature (T_B) and a transition temperature from low to high martensitic phases (T_C^M) was revealed.

Before the measurements the sample was cooled in zero field strength from T = 350 K to T = 5 K before the field was switched on. Magnetization measurements were performed during heating (ZFC) and cooling (FC) in magnetic field of 100 Oe with T from 5 to 350 K, with 1 K step (See Fig. 19). Average heating and cooling temperature rate was 0.0099 K/s.

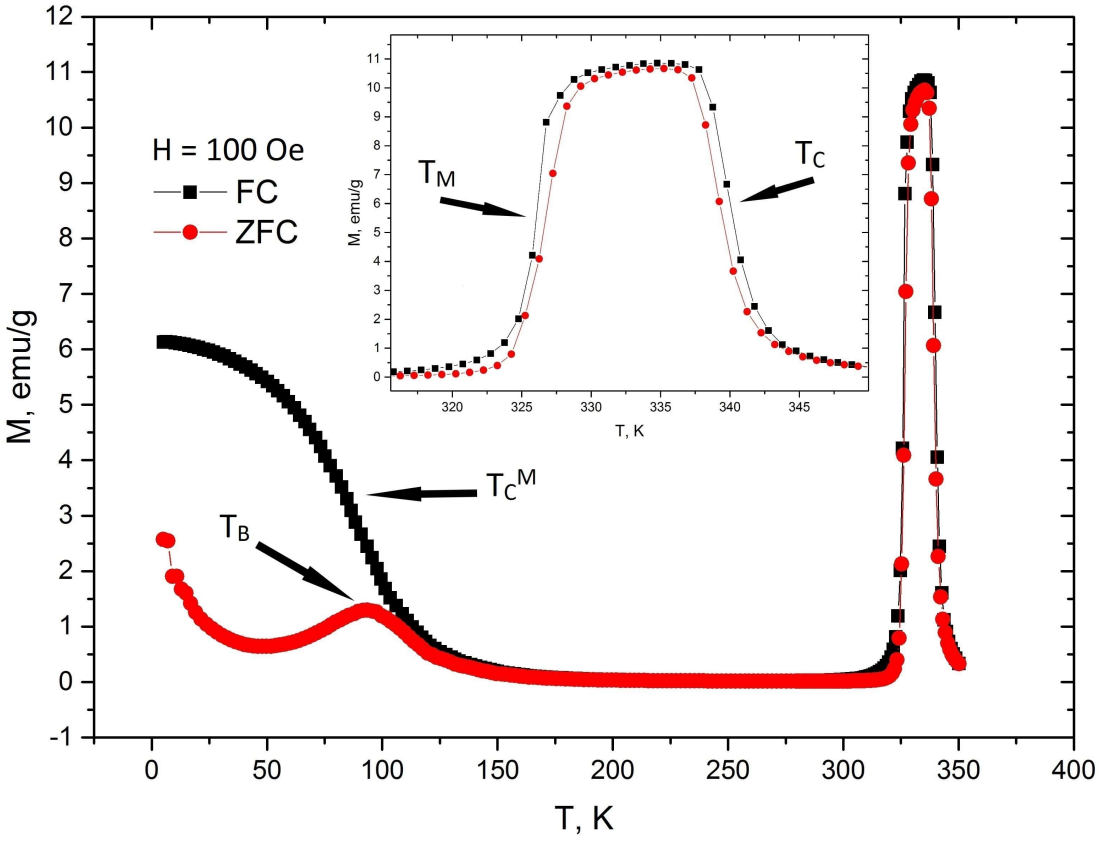

Figure 19. ZFC and FC magnetization as a function of temperature at H = 100 Oe with indicated transition temperatures.

As can be seen from the Fig. 19, abrupt magnetization change at T_M (the martensitic transition) separates two distinct regions. It is clear that thermal hysteresis exists, which means that we observe FOPT. However, the width of the hysteresis at such low field is relatively small ΔT < 1 K. The starting and ending temperatures of forward and inverse martensitic transition ($M_s \simeq A_s \simeq 324.5K$ and $M_f \simeq A_f \simeq 327K$) are comparable.

The sharp change of magnetization around T_C = 339 K (The Curie temperature of the austenitic phase) during cooling and heating is attributed to paramagnetic-ferromagnetic transition. The gradient near the Curie temperature of MP (T_C^M) is second order phase transition from low to high MP temperature. Dissimilarity of ZFC and FC curves is attributed to AFM/FM exchange interaction, which leads to EB phenomenon described above (See Chapter 6). The magnetization growth at blocking temperature (T_B) near 100 K is associated with alignment of magnetic domains towards the magnetic field.

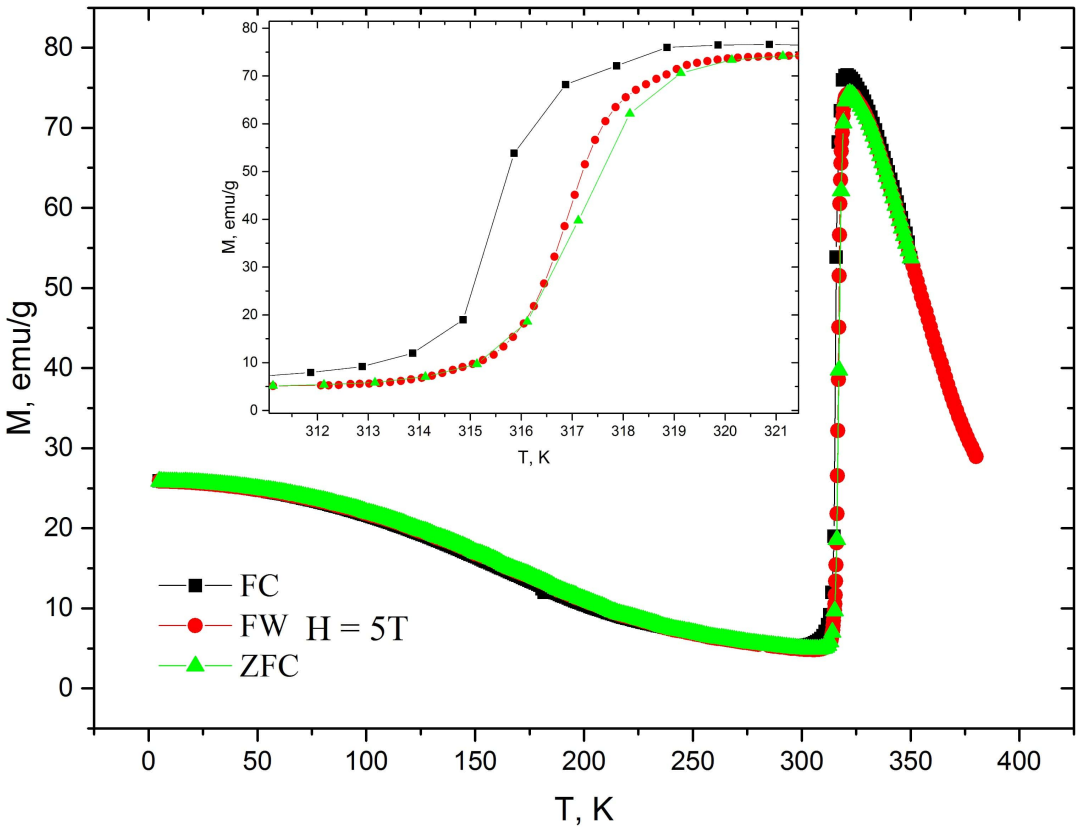

Figure 20. ZFC and FC magnetization as a function of temperature at H = 5 T.

The Figure 20 demonstrates temperature dependence (TD) at H = 5 T. Unlike the first measurements, this dependence contains second heating (FW) after ZFC and FC. According to the graph, difference between FW and ZFC (they are both heating) is negligible (ΔT < 0.4 K). Another significant observation is martensitic transition shift due to field change. The hysteresis at H = 5 T is shifted in negative direction approximately by 9 K in comparison with TD at H = 100 Oe, starting and ending hysteresis temperatures are 315 and 319 K, respectively. In addition, the hysteresis width at H = 5 T was increased twice $\Delta T \simeq 1.8K$ in comparison with $\Delta T < 1K$ at H = 100 Oe. The difference in ZFC and FC magnetization at low temperatures is absent due to strong magnetic field, which

causes all magnetic moments to be aligned towards the field. The slope at $T > A_f$ is still steep but not almost vertical like in case of $M(T)$ at 100 Oe. This indicates the persistence of the magnetic ordering even at high temperatures due to strong external magnetic field.

The martensite to austenite transition was investigated by measuring the field dependences at temperatures which are close to the T_M. Starting from 270 K, the temperature was increased in steps of 10 K to 340 K. Magnetic field strength interval was from -6 to 6 T. After each temperature, a degaussing procedure was done, in order to remove residual magnetization of sample. Figure 21 illustrates the absence of hysteresis at temperatures from 270 to 310 K. This can be explained by the domination of the paramagnetic phase at these temperatures (See Fig. 1).

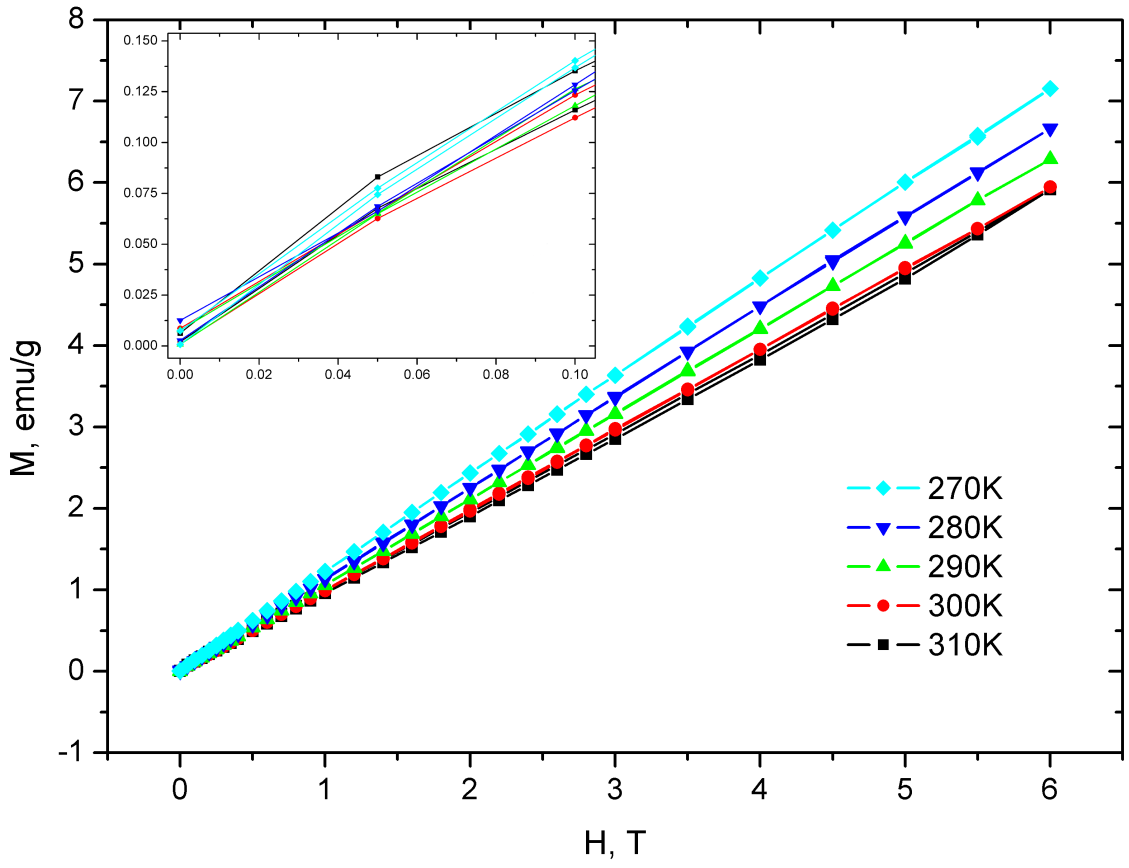

Figure 21. Field dependencies at temperature range from 270 to 310 K. Lines are guide for the eye.

However, at higher temperatures we can observe start of MT and genesis of FM phases (See Fig.22). Since the sample is in phase-mixed regime during the FOPT, some parts are in the FM phase, but other are still in the paramagnetic phase. At temperatures from 325 to 340 K, magnetization saturation was not achieved even at H = 6 T. The hysteresis at T = 315, 317 and 320 K have different width (See Fig. 23). As can be seen from the Fig. 22, the higher the temperature the lower start field strength of the hysteresis. This hysteresis is attributed to the magnetic field-induced martensitic transition. Therefore, the higher the temperature the bigger fraction of the material went through the transition, hence smaller field value is needed to transform the rest of the sample. Strangely, the magnetization in 6 T field at intermediate temperature of 317 K was on level of that at T = 325 K higher than magnetization at 320 K.

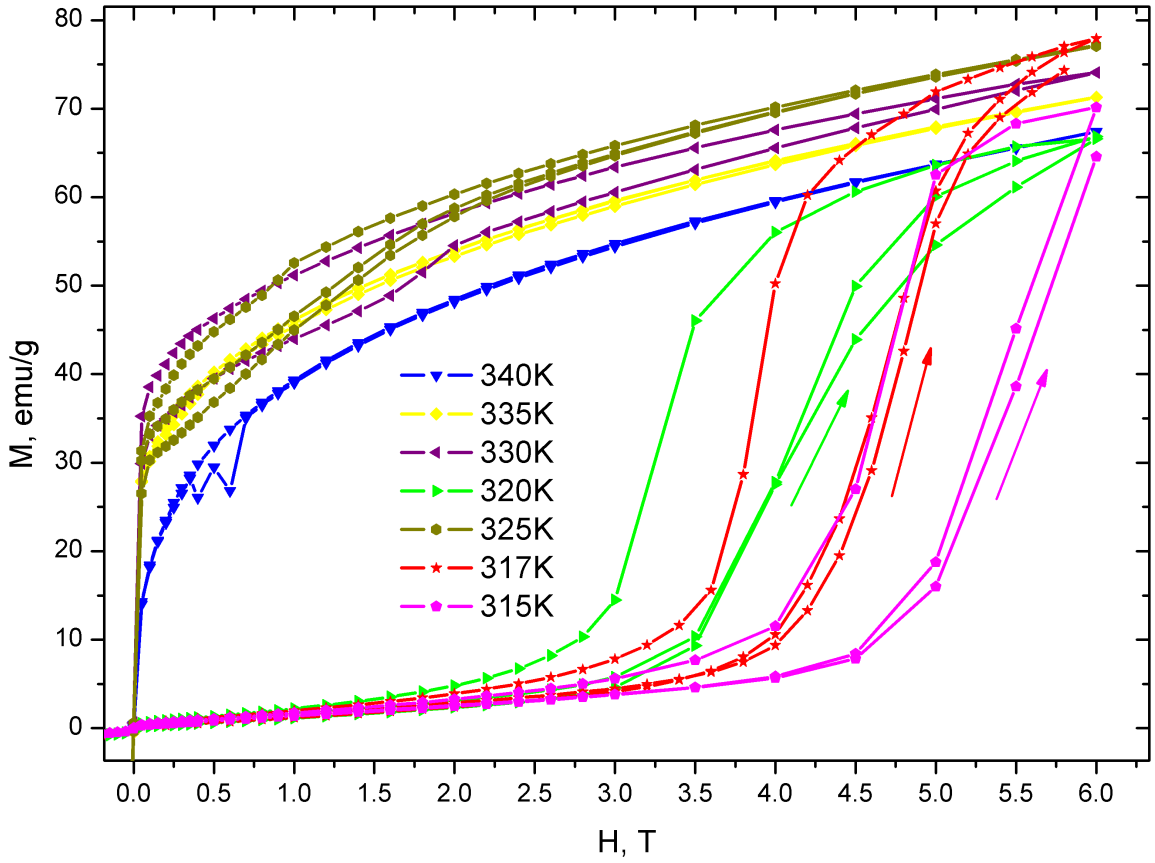

Figure 22. Field dependencies in the vicinity of the MT (from 315 to 340 K).

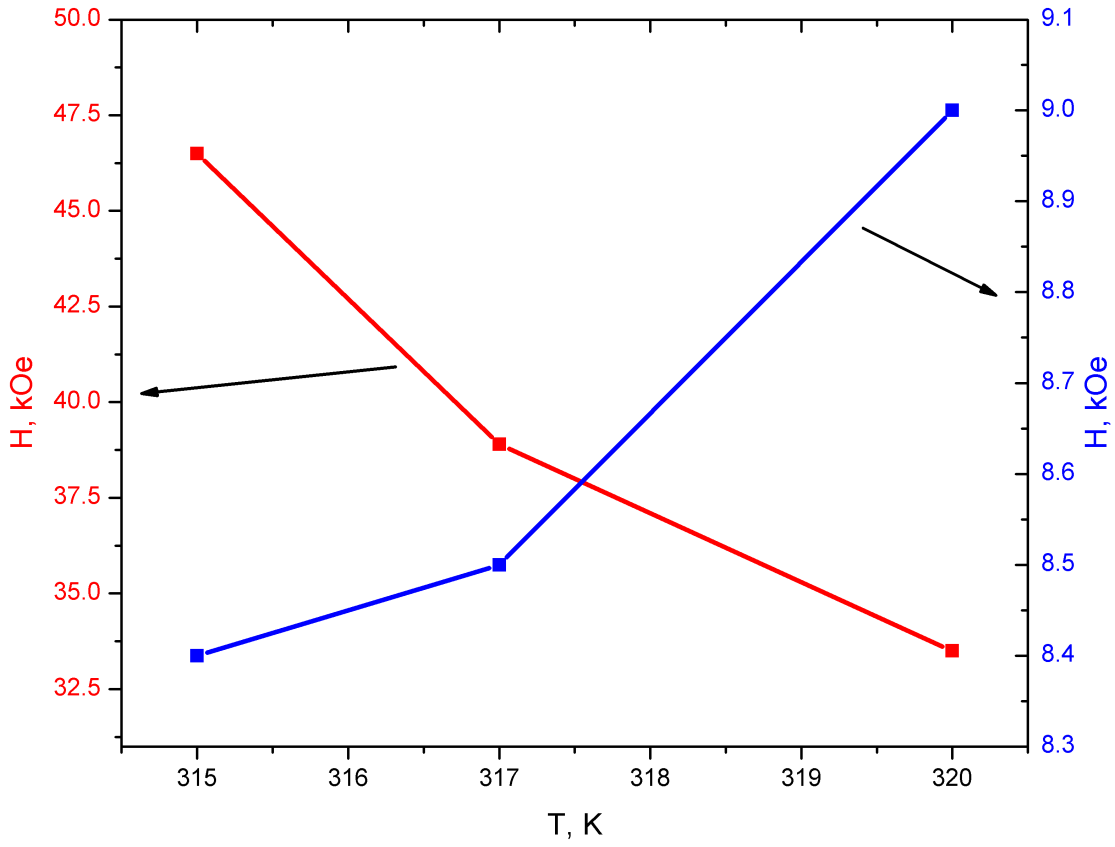

Figure 23. Temperatures dependencies of the field of the direct martensitic transition (left axis) and the hysteresis width (right axis).

In order to measure the hysteresis loop shift quantity, associated with exchange bias effect, the measurement was started after cooling from 350 to 5 K in the presence of H = 5 T. The start value of the magnetic field strength was 5 T. The cooling in the negative field value would cause shift in the opposite direction. The magnetic field saturation is observed at $H \approx 1$ T.

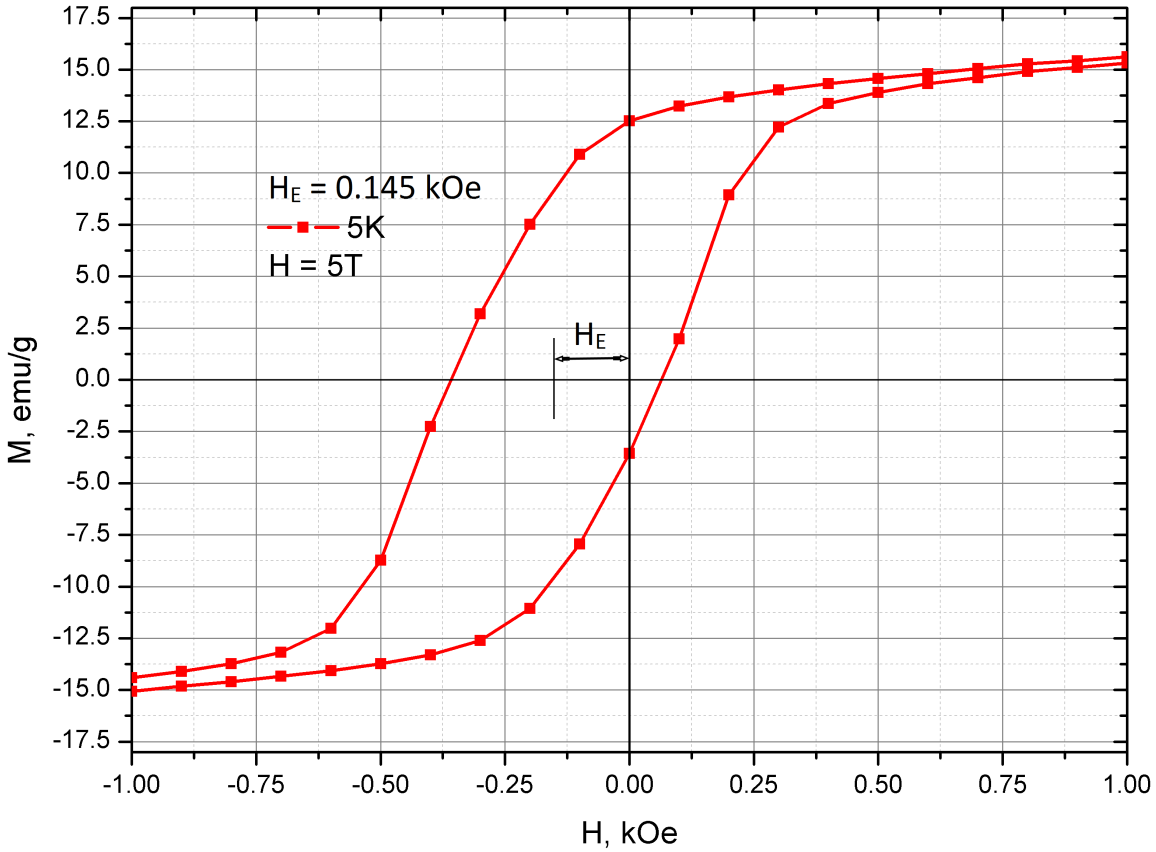

Figure 24. The field dependence measured at T = 5 K with the clear hysteresis loop shift. The H_E is evaluated as 145 Oe.

In terms of M (H) curves, the ΔS_m value was estimated using MATLAB software and "LakeShore Cryotronics" application note authored by V. Franco [4]. The code of calculation is presented below.

```
% Input data
mu0 = 1.256637E-6;   % [T * m / A]
mass = 1.8e-6;       % [kg]
load('M');           % [A * m2]
load('T');           % [K]
load('H');           % [T]

```

```
% CHOOSE the upper limit of integration Hmax in units of Tesla ...
    [0, 6]
Hmax = 4;            % [T]
jmax = find(H(:,1) ≥ Hmax,1);

% Variables
ΔSm_mid = zeros(1,length(T)-1);
T_mid = zeros(1,length(T)-1);
ΔSm_centr = zeros(1,length(T)-2);
T_centr = T(2:length(T)-1);

% Caculation
% middle point approach
for i = 1:length(T)-1
    for j = 1:jmax
        ΔSm_mid(i) = ΔSm_mid(i) + ...
            (M(j,i+1) - M(j,i))/(T(i+1) - T(i)) * (H(j+1) - H(j));
    end
    T_mid(i) = (T(i+1)+ T(i))/2;
end
ΔSm_mid = ΔSm_mid * mu0 / mass;


% central point approach
for i = 2:length(T)-1
    for j = 1:jmax
        ΔSm_centr(i-1) = ΔSm_centr(i-1) + ...
            (M(j,i+1) - M(j,i-1))/(T(i+1) - T(i-1)) * (H(j+1) - ...
               H(j));
    end
end
ΔSm_centr = ΔSm_centr * mu0 / mass;

% Combining the ΔSm data, first and last points
% are obtained by the 'middle point' approach and
% the intermediate points are from 'central point' approach
ΔSm_final = [ΔSm_mid(1,1), ΔSm_centr(1,:), ΔSm_mid(1,end)];
T_final = [T_mid(1,1), T_centr(1,:) T_mid(1,end)];
DeltaSm = [T_final' ΔSm_final'];
save('ΔSm.txt','DeltaSm','-ascii');
```

Fig. 25 shows calculated ΔS_m and indicates the coexistence of the direct and inverse MCE. The straight line over T = 275 - 290 K is associated to paramagnetic state of the sample. The negative value of ΔS_m from 300 to 315 K is attributed to martensitic transition from AP to MP and reaches its peak of -32.1 Jkg^{-1}K^{-1}. However, at higher temperatures ΔS_m changes its sign and rises abruptly to about 19.1 Jkg^{-1}K^{-1} that can be explained by ferromagnetic - paramagnetic transition at Curie point.

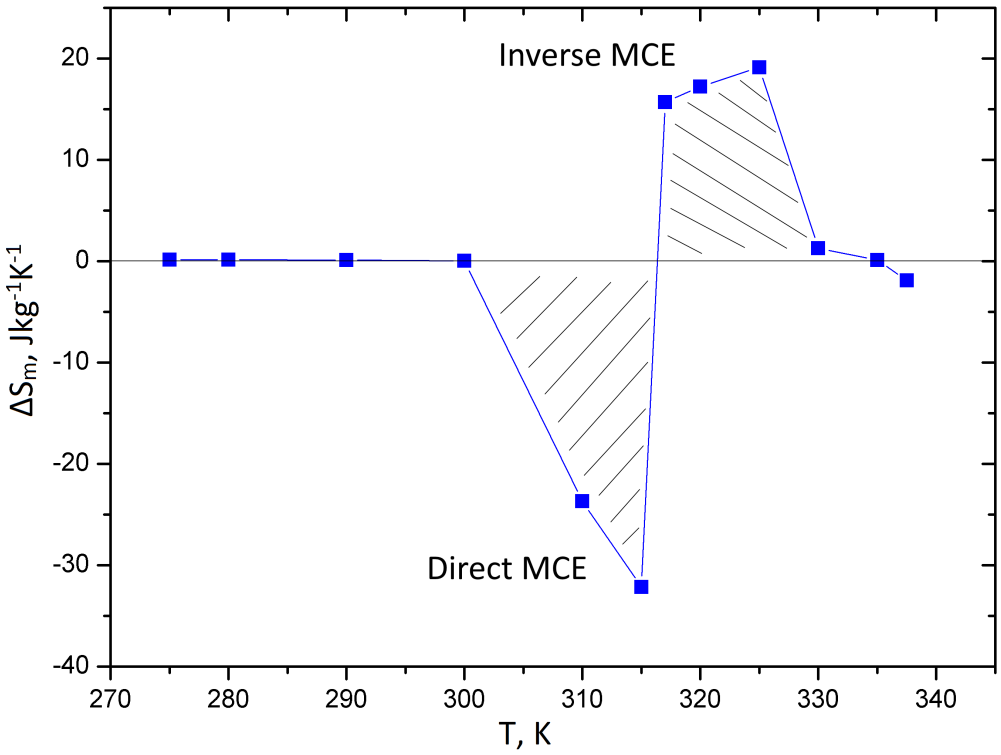

Figure 25. Magnetic entropy change as a function of temperature for a field change of ΔH = 6 T.

10 CONCLUSIONS

Using SQUID magnetometer, some magnetic properties of the $Ni_{48.5}Co_{1.5}Mn_{35}In_{15}$ Heusler alloy was studied. Following significant results, that are inherent in all Ni-Mn-based Heusler alloys, were obtained:

1. The sample undergo two main transitions: the first is between low-T martensitic and high-T austenitic phases (forward and inverse MT) and the second transition is between ferromagnetic and paramagnetic states at the Curie point.

2. Measurement results of the temperature dependencies at H = 100 Oe and 5 T helped to clarify transition phase temperatures (T_C^M, T_C, T_M), whose values can be tuned by the change in the magnetic field strength. Divergence of the magnetization curves, at temperatures below 150 K, reached its maximum value at 5 emu/g. At H = 5 T the hysteresis width is increased twice in comparison with measurements at H = 100 Oe. The magnetization change between the AP and MP reach the value of 11 emu/g over 324 - 327 K temperature range and 70 emu/g over T = 315 - 319 K range for H = 100 Oe and 5 T, respectively.

3. In order to calculate the ΔS_M, the field dependencies at temperatures of the MT vicinity was measured. The explicit hysteresis loop was determined in the field interval from 2.5 to 6 Tesla at three temperatures (T = 315, 317 and 320 K).

4. The exchange bias effect measured at T = 5 K is attributed to FM/AFM coexistence at low temperatures (described above curves divergence). The hysteresis shift value (H_E) is 145 Oe.

5. The magnetic entropy change achieves its peak of -32.1 $Jkg^{-1}K^{-1}$ for FOPT and 19.1 $Jkg^{-1}K^{-1}$ for SOPT with an external field increased from 0 to 6 T.

REFERENCES

[1] Lakhan Bainsla and K.G. Suresh. Equiatomic quaternary heusler alloys: A material perspective for spintronic applications. *Applied Physics Reviews*, 3(3):031101, 2016.

[2] Peter J. Webster. Heusler alloys. *Contemporary Physics*, 10(6):559–577, 1969.

[3] I. Galanakis, P.H. Dederichs, and N. Papanikolaou. Slater-pauling behavior and origin of the half-metallicity of the full-heusler alloys. *Physical Review B*, 66(17):174429, 2002.

[4] Victorino Franco. Determination of the magnetic entropy change from magnetic measurements.

[5] Josep Nogués and Ivan K. Schuller. Exchange bias. *Journal of Magnetism and Magnetic Materials*, 192(2):203–232, 1999.

[6] Arjun Kumar Pathak, Mahmud Khan, Igor Dubenko, Shane Stadler, and Naushad Ali. Large magnetic entropy change in $Ni_{50}Mn_{50}$-x in x heusler alloys. *Applied physics letters*, 90(26):262504, 2007.

[7] Mahmud Khan, Igor Dubenko, Shane Stadler, and Naushad Ali. Exchange bias in bulk Mn rich Ni–Mn–Sn heusler alloys. *Journal of Applied Physics*, 102(11):113914, 2007.

[8] Igor Dubenko, Tapas Samanta, Arjun Kumar Pathak, Alexandr Kazakov, Valerii Prudnikov, Shane Stadler, Alexander Granovsky, Arcady Zhukov, and Naushad Ali. Magnetocaloric effect and multifunctional properties of Ni–Mn-based heusler alloys. *Journal of Magnetism and Magnetic Materials*, 324(21):3530–3534, 2012.

[9] S. Tikadzumi. Physics of ferromagnetism. *Magnetic Characteristics and Practical Applications*, 1983.

[10] Sōshin Chikazumi. *Physics of magnetism*. Wiley, 1964.

[11] G.S. Krinchik. Physics of magnetic effects. *Moscow State Univ., Moscow*, 1976.

[12] C.M. Hurd. Varieties of magnetic order in solids. *Contemporary Physics*, 23(5):469–493, 1982.

[13] E.C. Stoner and E.P. Wohlfarth. A mechanism of magnetic hysteresis in heterogeneous alloys. *IEEE Transactions on Magnetics*, 27(4):3475–3518, 1991.

[14] Madan Rao, H.R. Krishnamurthy, and Rahul Pandit. Magnetic hysteresis in two model spin systems. *Physical Review B*, 42(1):856, 1990.

[15] E.S. Borovik, V.V. Eremenko, and A.S. Milner. Lectures on magnetism. *Fizmatlit, Moscow*, 2005.

[16] E.Z. Meilikhov and R.M. Farzetdinova. Exchange bias of hysteresis loop in the ising two-dimensional ferromagnet-antiferromagnet structure. *Journal of Experimental and Theoretical Physics*, 100(6):1112–1120, 2005.

[17] S.V. Vonsovskij. *Magnetizm: magnitiye svojstva dia-, para-, ferro-, antiferro-, i ferrimagnetikov*. Nauka, 1971.

[18] Iosif Galanakis. Theory of heusler and full-heusler compounds. In *Heusler Alloys*, pages 3–36. Springer, 2016.

[19] S. Soni, S. Dalela, S.S. Sharma, E.K. Liu, W.H. Wang, G.H. Wu, M. Kumar, and K.B. Garg. Study of electronic structure and magnetic properties of epitaxial Co_2FeAl heusler alloy thin films. *Journal of Alloys and Compounds*, 674:295–299, 2016.

[20] S.E. Kulkova, S.V. Eremeev, Tomoyuki Kakeshita, S.S. Kulkov, and G.E. Rudenski. The electronic structure and magnetic properties of full-and half-heusler alloys. *Materials transactions*, 47(3):599–606, 2006.

[21] Tanja Graf, Claudia Felser, and Stuart S.P. Parkin. Simple rules for the understanding of heusler compounds. *Progress in solid state chemistry*, 39(1):1–50, 2011.

[22] Y. A. Izyumov and V. N. Syromyatnikov. *Phase transitions and crystal symmetry*, volume 38. Springer Science & Business Media, 2012.

[23] A. M. Tishin and Y. I. Spichkin. *The magnetocaloric effect and its applications*. CRC Press, 2016.

[24] Iu M Gufan. Structural phase transitions. *Moscow Izdatel Nauka*, 1982.

[25] E.A. Zavadskii and V.I. Valkov. Magnetic phase transitions. *Kiev, Naukova Dumka*, 1980.

[26] O. Tegus, E. Brück, L. Zhang, K.H.J. Buschow, F.R. De Boer, et al. Magnetic-phase transitions and magnetocaloric effects. *Physica B: Condensed Matter*, 319(1):174–192, 2002.

[27] S. Yu Dan'Kov, A.M. Tishin, V.K. Pecharsky, K.A. Gschneidner, et al. Magnetic phase transitions and the magnetothermal properties of gadolinium. *Physical Review B*, 57(6):3478, 1998.

[28] T. Krenke, X. Moya, S. Aksoy, M. Acet, P. Entel, Ll Mañosa, A. Planes, Y. Elerman, A. Yücel, and E.F. Wassermann. Electronic aspects of the martensitic transition in Ni–Mn based heusler alloys. *Journal of Magnetism and Magnetic Materials*, 310(2):2788–2789, 2007.

[29] Yuri Mnyukh. The true cause of magnetostriction. *arXiv preprint arXiv:1103.4527*, 2011.

[30] Ivan Titov. *Influence of magnetism on the martensitic transition and related magnetocaloric effect in Ni-Mn-based Heusler alloys*. PhD thesis, Universitätsbibliothek Duisburg-Essen, 2015.

[31] Jafar Khalil-Allafi, Antonin Dlouhy, and Gunther Eggeler. Ni4ti3-precipitation during aging of NiTi shape memory alloys and its influence on martensitic phase transformations. *Acta Materialia*, 50(17):4255–4274, 2002.

[32] K. Oikawa, W. Ito, Y. Imano, Y. Sutou, R. Kainuma, K. Ishida, S. Okamoto, O. Kitakami, and T. Kanomata. Effect of magnetic field on martensitic transition of $Ni_{46}Mn_{41}In_{13}$ heusler alloy. *Applied physics letters*, 88(12):122507, 2006.

[33] C.M. Wayman. Shape memory alloys. *MRS bulletin*, 18(04):49–56, 1993.

[34] I. Dubenko, N. Ali, S. Stadler, A. Zhukov, V. Zhukova, B. Hernando, V. Prida, V. Prudnikov, E. Ganshina, and A. Granovsky. Magnetic, magnetocaloric, magnetotransport, and magneto-optical properties of Ni–Mn–In-based heusler alloys: bulk, ribbons, and microwires. In *Novel Functional Magnetic Materials*, pages 41–82. Springer, 2016.

[35] T. Tadaki, K. Otsuka, and K. Shimizu. Shape memory alloys. *Annual Review of Materials Science*, 18(1):25–45, 1988.

[36] V.A. Lvov, V.A. Chernenko, and J.M. Barandiaran. Magnetic shape memory materials with improved functional properties: Scientific aspects. In *Novel Functional Magnetic Materials*, pages 1–40. Springer, 2016.

[37] V.K. Pecharsky and K.A. Gschneidner Jr. Giant magnetocaloric effect in $Gd_5Si_2Ge_2$. *Physical review letters*, 78(23):4494, 1997.

[38] V.K. Pecharsky and K.A. Gschneidner Jr. Magnetocaloric effect from indirect measurements: magnetization and heat capacity. *Journal of Applied Physics*, 86(1):565–575, 1999.

[39] T. Kihara, X. Xu, W. Ito, R. Kainuma, and M. Tokunaga. Direct measurements of inverse magnetocaloric effects in metamagnetic shape-memory alloy Ni-Co-Mn-In. *Physical Review B*, 90(21):214409, 2014.

[40] Igor Dubenko, Mahmud Khan, Arjun Kumar Pathak, Bhoj Raj Gautam, Shane Stadler, and Naushad Ali. Magnetocaloric effects in Ni–Mn–x based heusler alloys with x = Ga, Sb, In. *Journal of Magnetism and Magnetic Materials*, 321(7):754–757, 2009.

[41] Arjun Kumar Pathak, Mahmud Khan, Bhoj Raj Gautam, Shane Stadler, Igor Dubenko, and Naushad Ali. Exchange bias in bulk Ni–Mn–In-based heusler alloys. *Journal of Magnetism and Magnetic Materials*, 321(8):963–965, 2009.

[42] Y. Fan, K.J. Smith, G. Lüpke, A.T. Hanbicki, R. Goswami, C.H. Li, H.B. Zhao, and B.T. Jonker. Exchange bias of the interface spin system at the Fe/MgO interface. *Nature nanotechnology*, 8(6):438–444, 2013.

[43] Feng-xia Hu, Bao-gen Shen, and Ji-rong Sun. Magnetic entropy change in $Ni_{51.5}Mn_{22.7}Ga_{25.8}$ alloy. *Applied Physics Letters*, 76(23):3460–3462, 2000.

[44] Cryogenic Limited. S700x squid magnetometer, user manual. pages 1–199, 2017.

[45] Tapani Ryhänen, Heikki Seppä, Risto Ilmoniemi, and Jukka Knuutila. Squid magnetometers for low-frequency applications. *Journal of Low Temperature Physics*, 76(5-6):287–386, 1989.

[46] C.D. Tesche. Superconducting magnetometers. *Cryogenics*, 29(12):1135–1142, 1989.

[47] Chao Jing, Jiping Chen, Zhe Li, Yanfei Qiao, Baojuan Kang, Shixun Cao, and Jincang Zhang. Exchange bias behavior and inverse magnetocaloric effect in $Ni_{50}Mn_{35}In_{15}$ heusler alloy. *Journal of Alloys and Compounds*, 475(1):1–4, 2009.